Civil Engineering and Applied Solutions

CEAS
Civil Engineering and Applied Solutions

Thermo-Mechanical Behavior of High-Strength Concrete with Nylon Granule Aggregates: Experimental Evaluation and Predictive Analysis

Fariborz Sasania [a], Mahdi Nematzadeh [a*], Maryam Asadi [a], Arman Aminian [a]

[a] Department of Civil Engineering, Faculty of Engineering and Technology, University of Mazandaran, Babolsar, Iran

A R T I C L E   I N F O

A B S T R A C T

In recent years, incorporating polymer trash as a substitute for natural aggregates in cementitious material has emerged as a sustainable approach to minimize environmental impact. Despite growing interest, limited studies have addressed the mechanical and microstructural performance of high-strength concrete (HSC) incorporating polymer waste under elevated temperature conditions. This research investigates the residual stress-strain response of HSC incorporating nylon granules (NG) as a partial substitute for natural sand at proportions of 0, 10, and 20%. Specimens were subjected to axial compressive loading after exposure to high temperatures of 20, 300, and 600°C. The analysis covered several physical and mechanical characteristics such as loss of weight, compressive strength, splitting tensile strength, elastic modulus, strain at peak stress, ultimate strain, toughness, stress-strain model, visual changes, and microstructure. The experimental findings were benchmarked against established codes and standards, including ACI 216, ASCE, EN 1994-1-2, EN 1992-1-2, and CEB-FIP. Results demonstrated that higher temperatures substantially impaired concrete performance, with compressive strength and modulus of elasticity declining by approximately 59% and 75%, respectively, at 600°C. Furthermore, the inclusion of NG led to additional reductions in mechanical performance. Based on the experimental observations, predictive models were formulated for mechanical properties, and a stress-strain model for NG-modified concrete was developed, which correlated well with the experimental results.

1. Introduction

Nowadays, with the growing global population, the consumption of both natural and non-natural resources is increasing significantly. As a result, human societies and the environment are facing the challenge of massive waste accumulation, which can lead to irreversible damage. Many researchers are striving to find effective ways to reduce the impact of these destructive activities or to identify suitable substitutes that cause less harm to the environment. In this context, polymer waste, particularly nylon bags, is considered one of the most damaging materials worldwide. A promising method for tackling environmental concerns involves repurposing waste materials by converting them into nylon granules (NG) through recycling processes, which can then serve as a partial substitute for natural aggregates in concrete [1]. Incorporating recycled NG into concrete not only reduces the reliance on natural resources but also results in a lighter composite material. This practice contributes to lowering the environmental footprint associated with excessive aggregate consumption. Additionally, the integration of recycled nylon materials into concrete can help alleviate pollution problems linked to discarded nylon products, such as bags [2]. Given the limited number of studies focusing on the application of recycled NG in concrete, this section reviews prior research on the behavior of concrete incorporating polymer-based waste. Tayebi and Nematzadeh [3], by examining the mechanical performance of concrete containing nylon granules at

* Corresponding author.
E-mail addresses: m.nematzadeh@umz.ac.ir (M. Nematzadeh).

replacement levels of 0, 10, and 20% of natural sand volume and reinforced with steel fibers at 0, 0.75, and 1.25%, under temperatures of 20, 300, and 600°C, demonstrated that increasing temperature results in significant degradation and reduction in the concrete's properties. The greatest decrease in compressive strength occurred after exposure to 600°C, with compressive strength and modulus of elasticity decreasing by 61 and 84%, respectively. In another study, Thomas and Chandra Gupta [4], investigating the performance of high-strength concrete (HSC) containing crumbed rubber for environmental benefits, reported that using crumb rubber (CR) particles as a partial substitute for concrete aggregates at volume fractions ranging from 0 to 20% is capable of producing concrete with compressive strengths of up to 60 MPa. On the other hand, Gupta et al. [5], in their investigation of the mechanical performance of rubber-containing concrete, showed that for 0.35, 0.4, and 0.55 water-to-cement (W/C) ratios, increased flowability of the fresh concrete was associated with improved compressive strength. In a study by Pelisser et al. [6], the effect of substituting 10% recycled rubber particles in HSC was reported, where only a 14% depletion in compressive strength was noticed compared to rubber-free concrete. Additionally, due to the lack of density of rubber aggregates, the specific weight of rubberized concrete decreased by 13% compared to ordinary concrete. Mousavimehr and Nematzadeh [7], through an experimental study on concrete incorporating crumb tire rubber exposed to high temperatures, reported that substituting 15% of natural fine aggregates with CR resulted in a 35% reduction in concrete specimens' compressive strength at ambient temperature compared to the control specimen. The greatest decrease in compressive strength was observed in the specimen with 30% CR content exposed to 400°C. Extensive studies at different replacement levels and particle sizes of crumb rubber have shown that, under a constant water-to-cement (W/C) ratio, increasing the amount of waste rubber particles leads to a drop in concrete specimens' compressive strength [8-10]. In this regard, Yilmaz and Degirmenci [11], investigating the effects of rubber aggregates on concrete, reported that all replacement levels of rubber aggregates used as a percentage of both fine and coarse aggregates leads to a drop in concrete compressive strength. However, increasing the particle size slightly decreased the water absorption of the concrete. Additionally, Nematzadeh and Mousavimehr [12], in their study on concrete containing CR and polyethylene terephthalate (PET) particles, reported that replacing 15% of natural aggregates with PET particles and 15% with CR led to a 40% drop in compressive strength relative to the control concrete specimens.

Nowadays, due to the significance of critical structures such as high-rise buildings, bridges, coastal structures, pavements, and industrial floors, high-strength concrete is widely used. HSC is a high-cement-content concrete with a dense internal structure and fine pores, typically produced using superplasticizers and silica fume powder [13]. The advantages of using HSC include improved compressive strength, reduced dead load, faster construction, and increased service life [14]. Singh et al. [15] conducted a study to evaluate the feasibility of using granite cutting waste (GCW) as a partial replacement for natural sand in HSC. The experimental results showed that replacing 25 to 40% of river sand with GCW positively affected compressive and flexural strength, abrasion resistance, permeability, and other durability indicators. The microstructural analysis confirmed these findings, revealing improvements in morphology and hydration processes within this replacement range. These results suggest that GCW is a sustainable material for partial sand replacement in concrete. In another study, Mohammad and Karim [16] investigated the impacts of using PET fibers on the mechanical behavior, initial crack impact resistance, and ultimate impact load capacity of HSC. PET fibers of varying lengths (10, 20, and 40 mm) and volume fractions (0.5, 0.75, 1.00, 1.25, and 1.5%) were added to the concrete, and 16 mix designs were tested. The findings indicated that using waste PET fibers can improve key properties of HSC and is recommended at up to 1.5% by volume

Since the fire resistance of structural elements, particularly reinforced concrete (RC) members, is a key consideration in the design, evaluating the mechanical properties of concrete during fire exposure is crucial [17]. Accordingly, much research has been organized on the behavior of concrete and RC members under high temperatures and the detrimental impacts of heat on their structural and mechanical performance [18, 19]. Most of these studies concluded that adding small amounts of rubber or polymer aggregates to concrete mixtures slightly reduces the risk of explosive spalling at elevated temperatures. In one such study, Karimi and Nematzadeh [20] explored how concrete-filled steel tube (CFST) columns behave when incorporating recycled tire rubber, particularly emphasizing their response to thermal exposure. This aspect has received limited attention in previous research, restricting the broader use of rubberized concrete in such structural elements. The study involved high-strength concrete (HSC) cores encased in seamless steel tubes subjected to various temperatures (20, 250, 500, and 750 °C). Key variables included the replacement rate of sand with recycled tire rubber (0, 5, and 10%), steel fiber content (0, 1, and 1.5%), and the diameter-to-thickness (D/t) ratio of the steel tubes (43 and 25.4). The findings indicated that a 10% rubber replacement led to a 12% reduction in the compressive strength of the confined specimens. However, thermal treatment did not significantly influence this strength reduction. Increasing steel fiber content and tube thickness improved the stiffness and enhanced the ductility trend in most specimens. The optimal steel fiber content was identified as 1%, which, while having minimal impact on compressive strength, significantly improved the ductility and energy absorption of the specimens, especially those exposed to elevated temperatures. Strength reduction was minimal up to 250 °C, but greater strength and post-peak stress-strain slope losses were observed at higher temperatures. In another study, Guo et al. [21] investigated the impacts of elevated temperatures on concrete containing crumb tire rubber reinforced with steel fibers. They reported that replacing natural fine aggregates with varying amounts of crumb tire rubber reduced mechanical behaviors such as compressive strength and modulus of elasticity at 200, 400, and 600°C. The average compressive strength reductions were approximately 25, 50, and 84% compared to reference concrete for each temperature, respectively. Nematzadeh et al. [22] investigated the behavior of concrete incorporating steel fibers and PET waste when exposed to high temperatures, reporting a significant drop in compressive strength for the PET-modified concrete relative to the control mix. The inclusion of steel fibers, however, enhanced mechanical performance, partially offsetting the thermal damage. In a separate study, Gupta et al. [23] examined concrete specimens with more than 10% natural aggregates substituted by rubber aggregates. They observed that after being subjected to 750 °C for two hours, the specimens experienced such extensive damage that compressive strength testing could not be

conducted. Marques et al. [24] reported that rubberized concrete with 5, 10, and 15% replacement of natural fine aggregates by recycled rubber particles exhibited compressive strength reductions of 64, 67, and 85%, respectively, after exposure to 400, 600, and 800°C, compared to normal concrete at room temperature. Al-Mutairi et al. [25] studied the effect of microsilica addition on the compressive strength of concrete containing coarse and fine rubber aggregates at elevated temperatures and found that rubberized concrete strength could improve at temperatures above 150°C with the inclusion of up to 5% microsilica. Mousa [26] investigated the impacts of crumb rubber aggregates on the behavior of concrete specimens exposed to 300, 400, 600, and 800°C for 120 minutes. After testing, many visible cracks were observed on the surface of specimens containing 5% rubber aggregates. Furthermore, the loss in compressive strength in rubberized concrete was more pronounced compared to reference concrete specimens. In the study conducted by Nematzadeh et al. [27], the effects of steel fibers and carbon fiber-reinforced polymer (CFRP) sheets on the post-fire bond behavior of steel rebars embedded in HSC containing waste polyethylene terephthalate (WPET) were investigated. The results showed that CFRP sheets positively impacted the rebar pull-out debonding energy, while steel fibers exhibited this positive effect only at 600 °C. On the other hand, steel fibers did not compensate for the negative influence of polymer aggregates and altered the failure mode at different temperatures. These fibers generally reduced bond strength under most conditions, although smaller rebar diameters mitigated this negative effect. In another study, Nematzadeh et al. [28] explored the influence of steel fibers and crumb rubber aggregates on the shear behavior of HSC beams reinforced with glass fiber-reinforced polymer (GFRP) bars aimed at reducing reinforcement congestion in areas with dense bar arrangements. Thirty beam specimens were cast to evaluate the effects of GFRP reinforcement ratio, shear span-to-depth ratio, crumb rubber content, and steel fiber volume fraction on shear performance. Results indicated that increasing fiber content, concrete compressive strength, and GFRP reinforcement ratio improved the beams' shear capacity while increasing the shear span-to-depth ratio and crumb rubber content reduced it. It was also found that steel fibers had a greater influence in enhancing shear performance at higher crumb rubber percentages, shifting from shear to flexural failure mode.

In light of the aforementioned studies, and aiming to better understand and predict the properties of HSC containing NG aggregates, this research investigates the mechanical behavior of HSC with nylon granules after experiencing elevated temperatures. To achieve this, compressive performance parameters such as compressive strength, strain at peak stress, elastic modulus, ultimate strain, and stress-strain curves were analyzed. The main variables include the volumetric replacement ratio of nylon granules for natural fine aggregate (0, 10, and 20%) and the exposure temperature (20, 300, and 600 °C). The obtained compressive strengths were compared with values estimated using design codes, including ACI 216 [29], ASCE [30], EN 1994-1-2 [31], EN 1992-1-2 [32], and CEB-FIP [33].

2. Research significance

High-strength concrete is widely used in critical and large-scale structures such as towers, bridges, and tunnels due to its superior mechanical properties. However, exposure to elevated temperatures during fire incidents can significantly reduce its strength and durability. To promote sustainable construction and address durability concerns, this research examines how elevated temperatures influence the mechanical behavior and microstructure of high-strength concrete containing nylon granules, which partially substitute natural fine aggregates. The study involves substituting a portion of natural sand with these granules and assesses their effects on compressive strength, splitting tensile strength, and elastic modulus both at room temperature and after exposure to high temperatures. Beyond mechanical and post-fire performance, the study emphasizes the environmental benefits of using recycled nylon granules, such as reducing dependency on natural aggregates and mitigating environmental degradation caused by excessive natural aggregate extraction. Incorporating plastic waste into concrete promotes sustainable construction practices, reduces environmental pollution, and supports economic principles. This study aims to contribute to the innovation of environmentally friendly and heat-resistant concrete, which can be highly beneficial for modern construction applications. The methodology of this study is illustrated in Fig. 1.
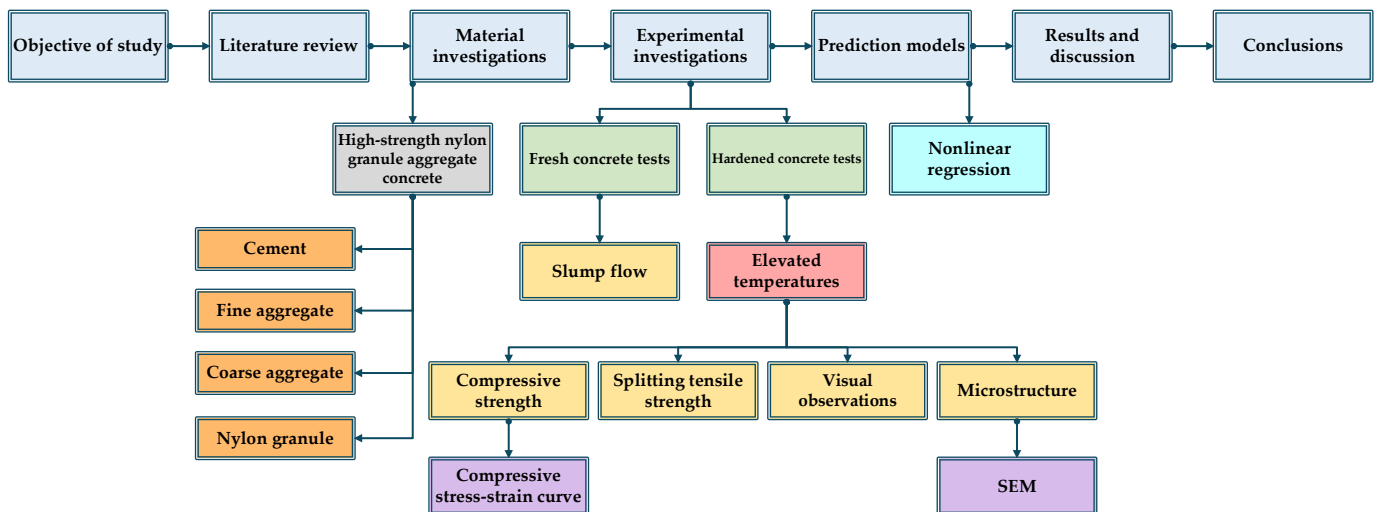

Fig. 1. Research methodology.

3. Experimental program

3.1. Material properties

This study used Type II Portland cement (CEM II/A-LL 42.5 N) compliant with ASTM C150 [34]. The physical and chemical properties of the cement composition provided by the manufacturer are presented in Table 1. Crushed dolomitic stone was used as the natural coarse aggregate, with a specific gravity of 2.66 gr/cm³, water absorption of 0.7%, and a maximum particle size of 12.5 mm. Additionally, natural fine aggregates with a fineness modulus of 2.77, a specific gravity of 2.63 gr/cm³, and a water absorption rate of 1.65% were used. Fig. 2 shows the particle size distribution of natural fine and coarse aggregates based on the requirements of ASTM C33 [35]. The percentage passing of aggregates through different sieves is presented in Table 2.

Table 1. Chemical, physical, and mechanical properties of Type II portland cement.

| Chemical properties		Type II portland cement (CEM II/A-LL 42.5 N)
		(wt.%)
Silicon dioxide (SiO_2)		20.7
Aluminium oxide (Al_2O_3)		5.2
Ferric oxide (Fe_2O_3)		4.6
Calcium oxide (CaO)		65
Magnesium oxide (MgO)		1.8
Sulfur trioxide (SO_3)		2.2
		0.5
Sodium oxide (Na_2O)		0.15
Free calcium oxide (Free CaO)		1.3
Loss on ignition (L.O.I)		1
Insoluble residue (In.R)		0.4
Tricalcium silicate (C_3S)		59.47
Dicalcium silicate (C_2S)		14.48
Tricalcium aluminate (C_3A)		6
Tetracalcium aluminoferrite (C_4AF)		14
Physical properties		**Type II portland cement (CEM II/A-LL 42.5 N)**
Autoclave expansion (%)		0.08
Specific surface (cm²/gr)		32
Initial setting time (min)		140
Final setting time (min)		240
Mechanical properties		**Type II portland cement (CEM II/A-LL 42.5 N)**
	3 days	26.47
Compressive strength (MPa)	7 days	43.14
	28 days	51.97
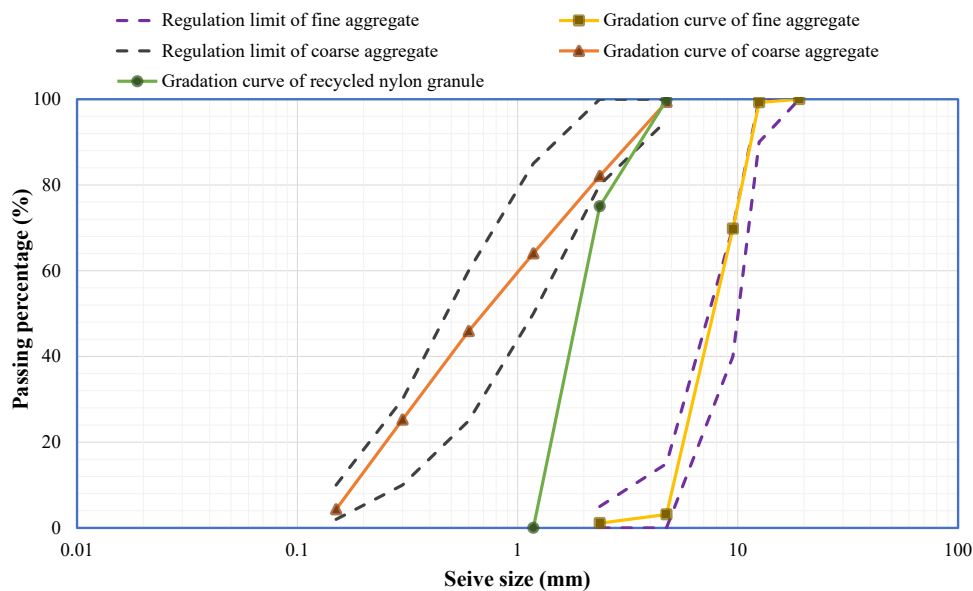
Fig. 2. Particle size distributions of fine and coarse aggregates according to ASTM C33 [35].

Table 2. Classification of aggregates.

Sieve size	Coarse aggregate		Sand aggregate		Nylon granule
	ASTM C33 [35] Min-Max	Passing percentage (%)	ASTM C33 [35] Min-Max	Passing percentage (%)	Passing percentage (%)
¾ inch (19 mm)	100	100	100	100	100
½ inch (12.5 mm)	90-100	99	100	100	100
3/8 inch (9.5 mm)	40-70	69	100	100	100
No. 4 (4.75 mm)	0-15	3	95-100	99	99
No. 8 (2.36 mm)	0-5	1	80-100	82	75
No. 16 (1.18 mm)	-	-	50-85	64	-
No. 30 (0.6 mm	-	-	25-60	45	-
No. 50 (0.3 mm)	-	-	5-30	25	-
No. 100 (0.15 mm)	-	-	0-10	4	-

In this study, granulated nylon particles were produced by recycling plastic nylon bags and subsequently used as a partial replacement for natural fine aggregates in the concrete mix. The size and shape of the NGs are shown in Fig. 3. The specific gravity of the NGs, determined according to ASTM C128 [36], was found to be 0.84. The thermal gravimetric analysis (TGA) curve for the NGs is presented in Fig. 4, which shows that the material loses approximately 90% of its mass at 600°C. It is also observed that the degradation temperature is 447.8°C. However, as a thermoplastic, the melting point of the nylon granules is significantly lower than their decomposition temperature. The silica fume powder used in this study was of type MK.A102 in powdered form. It was added to the concrete mix at 10% of the cement weight. Table 3 provides the chemical composition and physical properties of the micro-silica powder.

Fig. 3. Shape and dimensions of recycled nylon granules.

Table 3. Chemical and physical properties of silica fume.

| Chemical properties	Silica fume (MK.A102)
	(wt.%)
Silicon dioxide (SiO_2)	≤ 95
Aluminium oxide (Al_2O_3)	0.6
Ferric oxide (Fe_2O_3)	1.2
Calcium oxide (CaO)	0.5
Magnesium oxide (MgO)	0.6
Potassium oxide (K_2O)	0.4
Sodium oxide (Na_2O)	0.7
Loss on ignition (L.O.I)	1.5 – 2.5
Moisture	0.4
Physical properties	
Specific gravity (g/cm^3)	2.2
Specific surface (m^2/g)	15
Bulk density (kg/m^3)	350
Mean particle size (mic)	0.6
pH	8
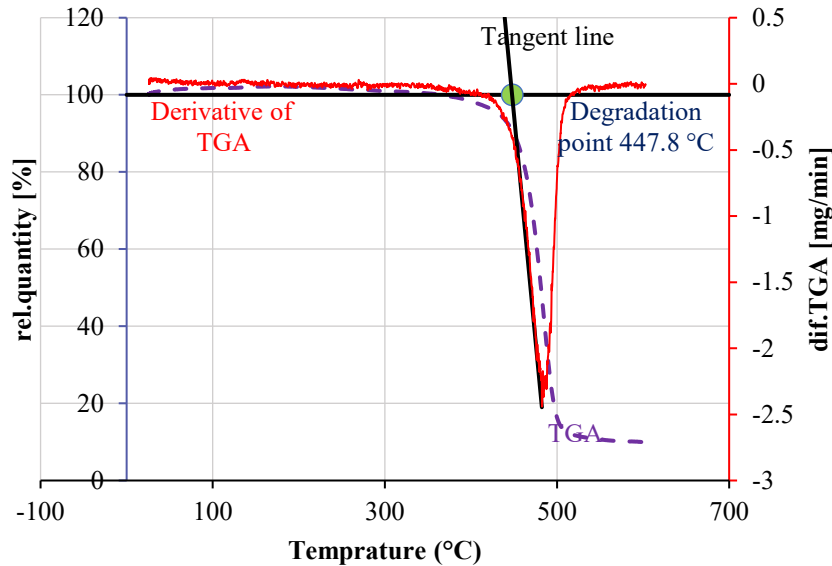
Fig. 4. Thermal gravimetric analysis (TGA).

In this study, a polycarboxylate ether–based superplasticizer (SP), commercially known as PCE–SR5, with a solid content of 42% and a specific gravity of 1.03 gr/cm³, was used in all concrete mix designs at 0.8% by mass of cement. The superplasticizer was employed to improve the dispersion of pozzolanic materials throughout the concrete mix, achieve good workability, and enhance both early and final compressive strengths. The properties of the superplasticizer additive are presented in Table 4.

Table 4. Superplasticizer properties.

Name	Appearance	Chemical mixture	Ionic nature	PPM	Density	Freezing temperatures
PCE-SR5	Light brown liqued	Modified polycarboxylic acid copolymers	Anionic	500 MAX	1.03 g/cm³	About -2ºC

3.2. Concrete mix design and specimen preparation

This study developed three mix designs for high-strength concrete HSC incorporating nylon granules, as presented in Table 5. To prepare the concrete, natural coarse and fine aggregates were first mixed in a concrete mixer for 1 minute. Then, cement and silica fume powder were added and mixed for an additional minute. Afterward, a premixed solution of water and superplasticizer was gradually introduced into the mixer and blended with the dry materials for 3 minutes. In the mixes containing nylon granules, these particles were added to the mixer along with the natural aggregates. A total of 54 cylindrical concrete specimens with a diameter of 100 mm and a height of 200 mm were cast to evaluate the compressive behavior of HSC containing NG after exposure to elevated temperatures. To minimize experimental error, three identical specimens were prepared and tested for each group. The three mix designs incorporated nylon granules as a partial volumetric replacement for natural fine aggregates at 0, 10, and 20% replacement levels. A constant water-to-cement ratio (W/C) of 0.31 was used across all mixes. The mix proportions per cubic meter were determined in accordance with ACI 211.1 [37] and are detailed in Table 5.

Table 5. Proportions of mix components.

Mix No.	Mix ID	Coarse agg.	Fine agg.	Nylon granule	Cement	Silica fume	Water	W/C	SP* (%)	Slump (mm)
		(kg/m³)								
1	HSC-NG0®	951	437	0	564	63	212	0.31	0.8	80
2	HSC-NG10	951	379	14	564	63	212	0.31	0.8	100
3	HSC-NG20	951	321	28	564	63	212	0.31	0.8	110

* Percentage of total weight of cementitious material.

In this study, the slump test was conducted to evaluate the workability and flowability of fresh concrete in accordance with ASTM C143 [38]. The procedure involved placing the fresh concrete into a slump cone in three layers. Each layer was compacted with 25 blows using a tamping rod to ensure uniformity and eliminate air voids. Subsequently, the cone was lifted vertically, and the fresh concrete slump was determined by comparing the settled concrete's height to the cone's height. It is important to note that the tamping rod penetrated into the underlying layers during compaction. As mentioned in Table 5, a specific amount of superplasticizer was added to each mix to ensure proper workability. The measured slump values ranged from 80 to 110 mm. It was observed that the workability and flowability of the fresh concrete increased with the NGs addition. This improvement is attributed to the deformability and non-absorbent nature of nylon granules compared to natural sand. After casting, the concrete was compacted using a vibrating table to further reduce air entrapment and enhance homogeneity. All mixing, casting, and testing procedures were performed at a room temperature of 20°C. After 48 hours, the concrete specimens were demolded according to ASTM C192 [39].

The demolded specimens were then cured in a lime-saturated water solution for a minimum of 27 days, also in accordance with ASTM C192 [39].

For identification purposes, codes were assigned to each concrete mix. As shown in Table 5, "NG0" represents the control high-strength concrete with no nylon granules, while the numbers following "NG" indicate the percentage of nylon granules used as a volumetric replacement for natural fine aggregate. For heat-exposed specimens, additional labels such as T20, T300, and T600 were added to the codes, indicating the temperature in °C to which the specimens were subjected. For example, "HSC-NG20-T600" refers to a high-strength concrete specimen containing 20% nylon granules exposed to a high temperature of 600°C. A selection of hardened manufactured concrete cylinder specimens is shown in Fig. 5.

Fig. 5. A view of some hardened concrete specimens.

3.3. Thermal exposure

Each concrete mix group was subjected to three temperature levels: 20°C (ambient temperature), 300°C, and 600°C, with the latter two representing elevated temperature conditions. Thermal exposure was carried out using an electric furnace. Prior to exposure, all specimens were pre-heated at 60°C for 24 hours in accordance with ISO 834 [40] to remove surface moisture and ensure uniform initial conditions. Immediately after reaching 60°C, the specimens were heated to the target temperatures of 300°C and 600°C. The specimens were maintained at each target temperature for 1 hour. Following thermal exposure, the furnace vents were partially opened to accelerate cooling, and the specimens were left inside the furnace until they reached ambient temperature. During the heating process, thermocouples installed on the furnace's interior walls recorded the furnace temperature, while additional thermocouples embedded in the center of the specimens measured the concrete's internal temperature. Fig. 6 illustrates the time-temperature curve for both the specimen core and furnace environment at 300 and 600°C.
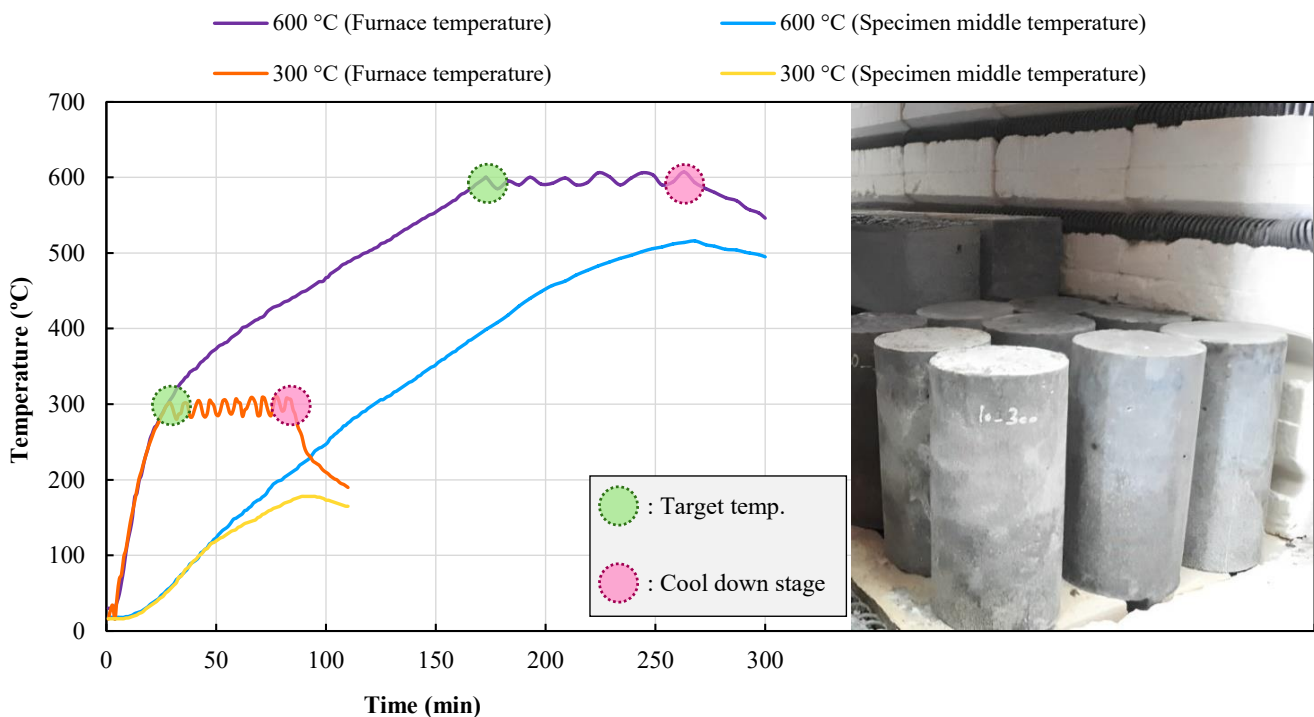

Fig. 6. Temperature variations in and out of concrete specimens.

Due to moisture loss and surface cracking caused by high temperatures, the concrete tends to reabsorb moisture from the environment upon cooling and removal from the furnace. This post-exposure rehydration leads to volumetric expansion and increased crack widths, ultimately reducing the heat-exposed specimens' mechanical strength. According to literature studies [41, 42], the specimens were stored at room temperature for a minimum of 10 days before mechanical testing to stabilize moisture content and microstructure. This procedure aligns with ACI 216 [29], which recommends a minimum post-exposure conditioning period of six days. After this period, compressive and splitting tensile strength tests were conducted under axial loading conditions. The overall procedure for specimen preparation and their exposure to elevated temperatures is illustrated in Fig. 7.
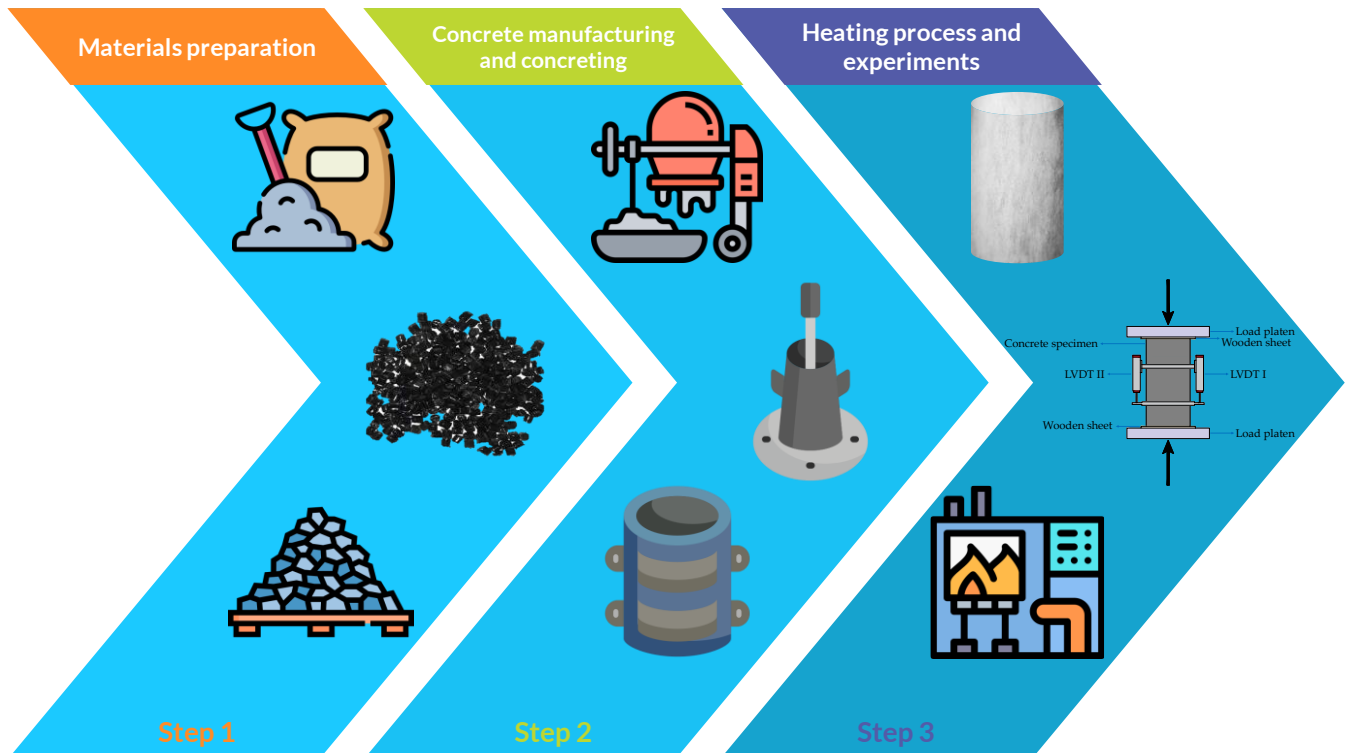
Fig. 7. High-strength nylon granule aggregate concrete manufacturing steps.

3.4. Testing Procedure

3.4.1.Compressive strength test

After 28 days of curing, the concrete cylindrical specimens were evaluated for compressive strength according to ASTM C39 [43], following the procedures outlined in ASTM C192 [39]. The testing apparatus used in this experiment, along with the concrete cylindrical specimen (100×200 mm), is shown in Fig. 8. The standard loading rate is within the range of 0.2 MPa/s to 0.3 MPa/s, and in this study, a loading rate of 0.25 MPa/s was used for the cylindrical specimens. Two thin wooden sheets were used to prevent stress concentration caused by the surface roughness of the specimens and achieve better axial compressive load distribution. As illustrated in Fig. 8, the cylindrical specimen's axial deformation was measured using two Linear Variable Differential Transformers (LVDTs), which were symmetrically attached to the specimen using a setup consisting of two steel rings. The final data for axial deformation were obtained by averaging the readings from the two LVDTs. The data related to load and displacement were used to plot the axial compressive stress-strain curve for the HSC cylindrical specimens containing NGs, both before and after exposure to elevated temperatures.

3.4.2.Splitting tensile strength test

After 28 days of curing the concrete cylindrical specimens in accordance with ASTM C192 [39], the splitting tensile strength test was conducted on the concrete cylinders based on ASTM C496 [44]. The standard loading rate ranges from 0.7 MPa/min to 1.4 MPa/min, and in this study, a loading rate of 1.15 MPa/min was used for the concrete cylindrical specimens. Similar to the compressive strength test, a thin wooden sheet was placed at the loading surface to ensure uniform load distribution.

3.4.3.Modulus of elasticity test

The initial elastic modulus of the concrete cylindrical specimens was determined from the slope of the axial compressive stress-strain curve at the beginning of axial compressive loading. Therefore, two LVDTs were used to obtain deformation data alongside the load measurements to plot the stress-strain curve. Additionally, the secant modulus of elasticity was determined according to ASTM C469 [45], using the chord slope drawn on the stress-strain curve between the strain point of 50 $\mu\varepsilon$ and the stress level corresponding to 40% of the material's compressive strength.
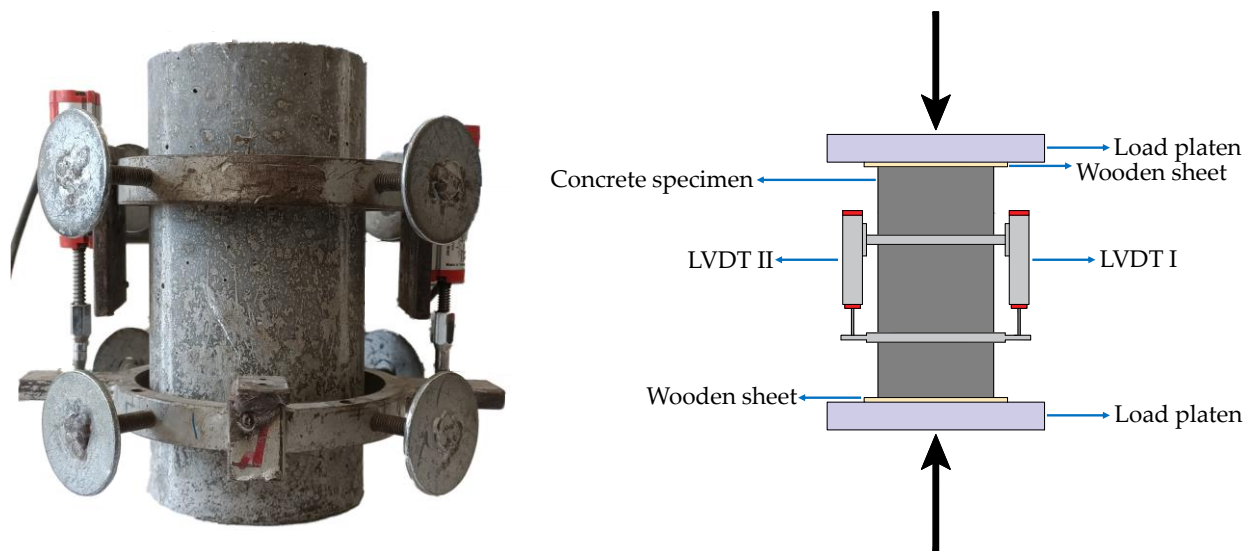
Fig. 8. Axial compressive stress–strain test setup.

4. Results and discussion

4.1. Loss of weight

High temperatures can have severely detrimental effects on the mechanical properties and durability of concrete specimens. One such effect is the weight loss of concrete specimens after exposure to elevated temperatures. This is particularly significant in the present study, as nylon granules with a decomposition temperature of 447.8 °C were used in the specimen preparation. According to the thermal gravimetric analysis curve presented in Fig. 4, nylon granules lose approximately 90% of their mass at 600 °C. Therefore, the specimens were weighed before and after the heat treatment and the weight loss percentage was calculated. The percentage of weight loss is presented in Fig. 9, which shows that the weight loss increases with rising temperature. As illustrated in Fig. 9, the specimens exposed to 300 and 600 °C exhibited approximately 2 and 8% weight loss, respectively, compared to the reference specimens (at ambient temperature). The weight loss at 300 °C is primarily attributed to the evaporation of surface and physically bound water from the concrete specimens after exposure to high temperatures [46-48]. Additionally, the water within the calcium silicate hydrate (C-S-H) gel begins to be released at around 150 °C, marking the initial stage of C-S-H decomposition. As the temperature increases to about 300 °C, a significant reduction in specimen weight is observed. This is mainly due to the decomposition of calcium hydroxide (CH) crystals, continued release of water from the C-S-H gel, evaporation of water from capillary pores, partial decomposition of nylon granules, and the release of physically absorbed water. Upon further temperature increase to 600 °C, there is a sharp decline in specimen weight. This notable reduction is due to the near-complete decomposition of the nylon granules within this temperature range. Given that the decomposition temperature of nylon granules is approximately 447.8 °C, at 600 °C, the granules decompose entirely and evaporate through the existing pores and microcracks in the concrete. The weight loss was such that, compared to specimens exposed to 20 °C, those with 10% nylon granule replacement experienced approximately 3 and 10% weight loss at 300 and 600 °C, respectively, and specimens with 20% nylon replacement showed approximately 4 and 11% weight loss at the same temperatures. Overall, the specimens without nylon replacement at room temperature and those with 20% nylon replacement at 600 °C exhibited the lowest (approximately 2%) and highest (approximately 11%) weight loss, respectively.

4.2. Compressive strength

Compressive strength in concrete materials is one of the most critical criteria for evaluating their mechanical performance. The compressive strength results of all high-strength concrete HSC cylindrical specimens containing NG exposed to elevated temperatures are presented in Fig. 10 and Table 6. According to Table 6, the compressive strength of HSC specimens containing NG, before and after exposure to high temperatures, ranged approximately from 21 MPa to 83 MPa. As shown in Fig. 10, the reference specimen without nylon granules at room temperature had the highest compressive strength. On the other hand, the results indicate that replacing 10 and 20% of natural fine aggregate with NG in unheated specimens led to a reduction in compressive strength of 25.2 and 59.2%, respectively. These findings show that including nylon granules reduces compressive strength, with the most significant reduction observed in specimens where 20% of the natural fine aggregate was replaced with NG. This decrease in strength is attributed to the fact that nylon granules are much softer and more flexible than natural fine aggregates when in contact with cement paste. As a result, cracks form more readily around the NG particles under axial compressive loading, weakening the material. Another contributing factor to the reduction in compressive strength could be the insufficient bond between the ductile nylon granules and the cement paste, leading to stress concentrations in the interfacial transition zone (ITZ) [49]. Compared to natural aggregates, nylon granules are more deformable and have smoother surfaces, behaving like voids within the concrete matrix. Additionally, NG has a lower density than natural fine aggregates, which disrupts the overall structure of the concrete aggregates and ultimately contributes to the reduction in compressive strength.
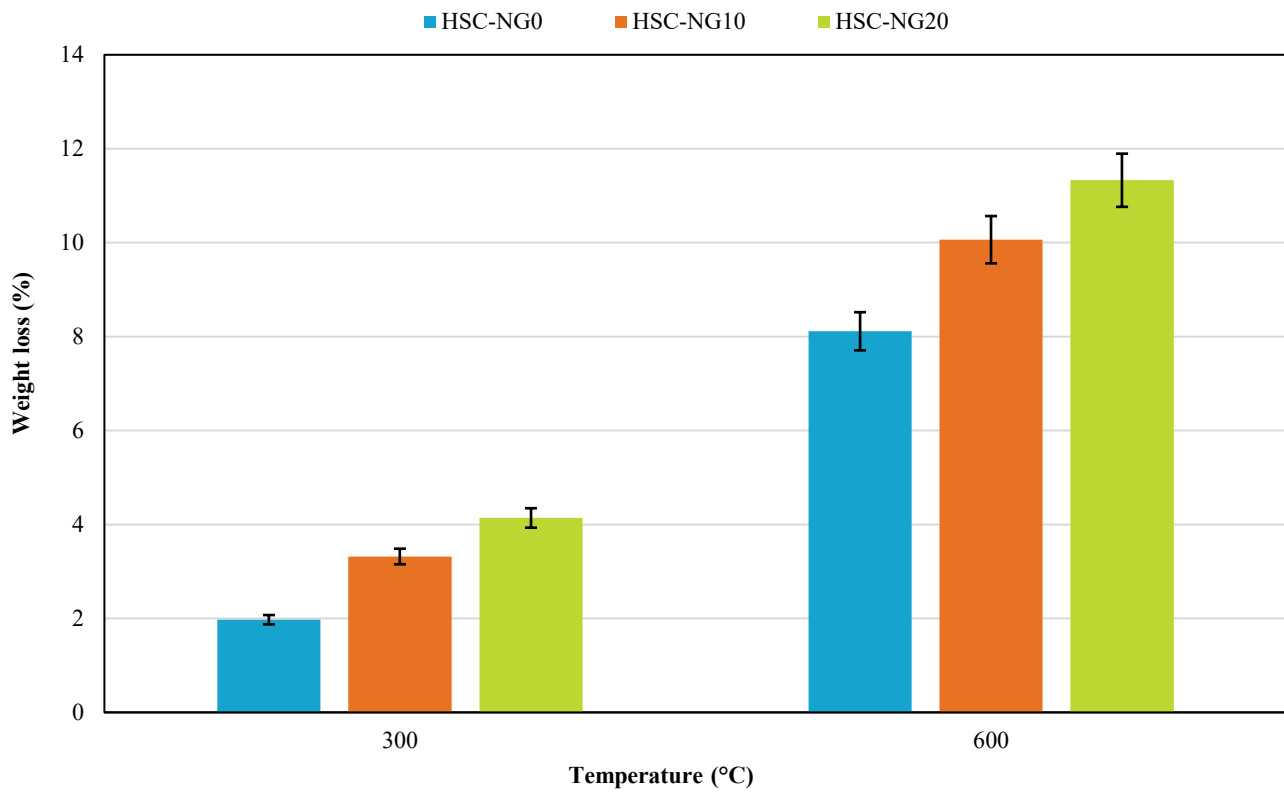
Fig. 9. Percentage of specimen weight loss in terms of elevated temperatures.

After exposure to high temperatures, the compressive strength of all groups significantly decreased. For instance, applying a temperature of 300 °C to specimens without NG resulted in a 25.2% reduction in strength compared to the same specimens at 20 °C. This reduction can be attributed to the loss of free and chemically bound water in the C-S-H gel, which leads to internal stresses and surface microcracking [50]. Furthermore, the compressive strength reductions for specimens HSC-NG0, HSC-NG10, and HSC-NG20 after exposure to 300 °C, compared to their counterparts at 20 °C, were 25.2, 12.2, and 11%, respectively. The majority of compressive strength loss occurred between 20 and 300 °C. In contrast, in the temperature range of 300 to 600 °C, the reductions in compressive strength for specimens HSC-NG0, HSC-NG10, and HSC-NG20 were 59.2, 65.2, and 63.6%, respectively, compared to those at 20 °C. Based on these results, specimens with 20% NG replacement exhibited less compressive strength loss at room temperature compared to the other groups. In addition to the aforementioned causes, dehydration (i.e., evaporation of chemically bound water from CH) also plays a significant role in the reduction of strength. At 600 °C, the nylon granules exceed their melting point, causing them to shrink and lose up to 90% of their mass. This results in increased porosity in the concrete matrix and ultimately reduces the strength of heat-exposed concrete specimens [48, 51]. Overall, the results presented in Fig. 10 and Table 6 indicate that using NG reduces concrete compressive strength. Interestingly, this reduction is less severe for the 20% NG replacement than the 10% replacement at high temperatures. However, the compressive strength loss for specimens containing 10% NG appears to stabilize at temperatures above 300 °C. Moreover, using up to 10% NG replacement with natural fine aggregates seems to offer a suitable balance between environmental and structural performance goals.

Table 6. Mechanical properties experimental results of specimens at elevated temperatures.

Specimen ID	Temperature (°C)	Compressive strength (MPa)		Splitting tensile strength (MPa)		Initial modulus of elasticity (GPa)		Secant modulus of elasticity (GPa)	
		Mean in MPa	CV (%)	Mean in MPa	CV(%)	Mean in GPa	CV (%)	Mean in GPa	CV (%)
HSC-NG0[®]	20	83.3 (-)	3.2	6.1 (-)	1.9	48.0 (-)	12.7	39.2 (-)	10.6
	300	62.3 (-)	1.0	5.0 (-)	7.0	44.7 (-)	11.3	34.8 (-)	8.7
	600	33.9 (-)	5.8	2.1 (-)	3.3	12.1 (-)	8.2	9.3 (-)	5.9
HSC-NG10	20	64.0 (-23.2 %)	3.4	4.9 (-19.7 %)	4.5	42.5 (-11.5 %)	9.3	33.5 (-14.5 %)	10.8
	300	56.2 (-9.8 %)	8.5	4.5 (-10 %)	11.4	41.3 (-7.6 %)	8.1	31.2 (-10.3 %)	11.0
	600	22.3 (-34.2 %)	9.4	2.0 (-4.8 %)	8.0	10.3 (-14.9 %)	7.6	8.14 (-12.5 %)	7.1
HSC-NG20	20	57.7 (-30.7 %)	2.3	4.6 (-24.6 %)	7.4	41.1 (-14.4 %)	8.9	31.2 (-20.4 %)	8.4
	300	51.4 (-17.5 %)	8.9	4.2 (-16 %)	7.3	38.1 (-14.8 %)	9.7	27.7 (-20.4 %)	8.8
	600	21.0 (-38 %)	3.0	1.6 (-23.8 %)	7.1	9.6 (-20.7 %)	9.1	7.8 (-16.1 %)	8.9

Note: The numbers in the parentheses show the percentage of increase or decrease in the concrete specimens' mechanical properties compared to the reference specimens (without nylon granule).
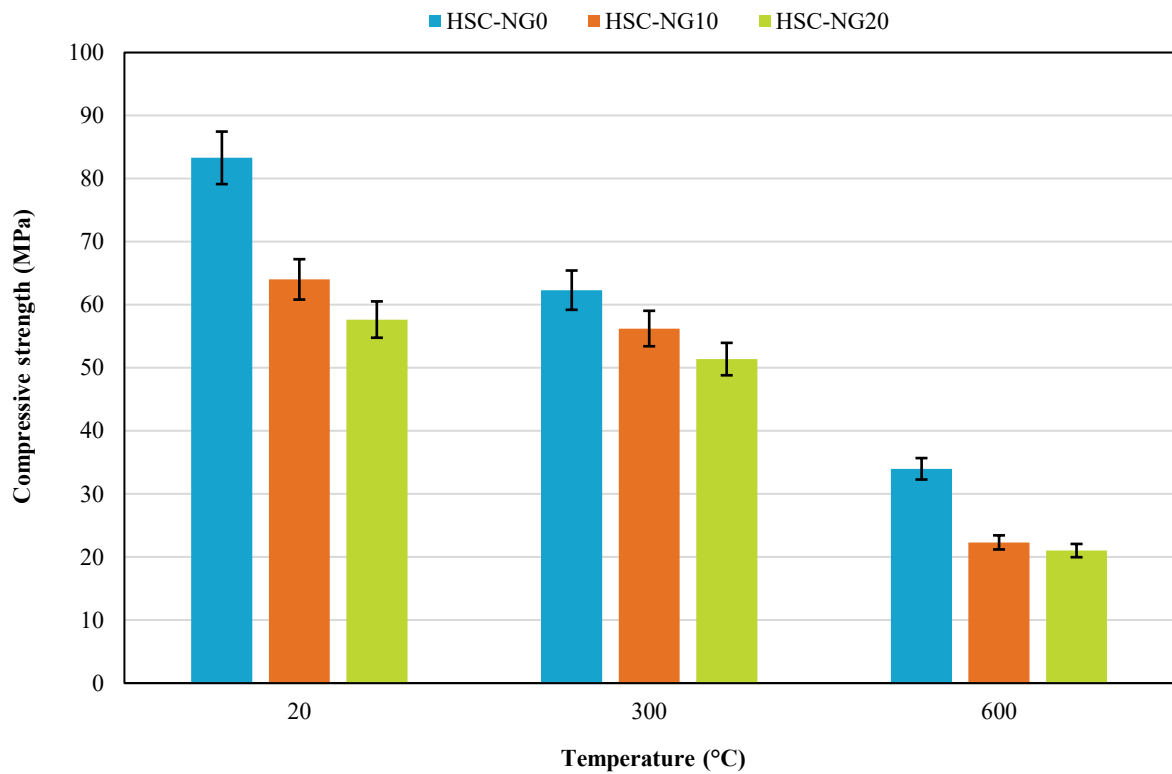
Fig. 10. Compressive strength of specimens before and after exposure to elevated temperatures.

The normalized compressive strength is defined as the ratio of the compressive strength of a specimen exposed to a target temperature ($f_{c(G,T)}$) to the compressive strength of the specimen at 20 °C ($f_{c(0,20)}$). Fig. 11 shows the values of normalized compressive strength as a function of temperature based on ACI 216 [29], ASCE [30] and EN 1994-1-2 [31]. This figure generally indicates that these codes provide reasonably accurate estimates of the normalized compressive strength values for the tested specimens. Furthermore, it appears that the presented experimental results closely align with the relationships proposed in the regulations.
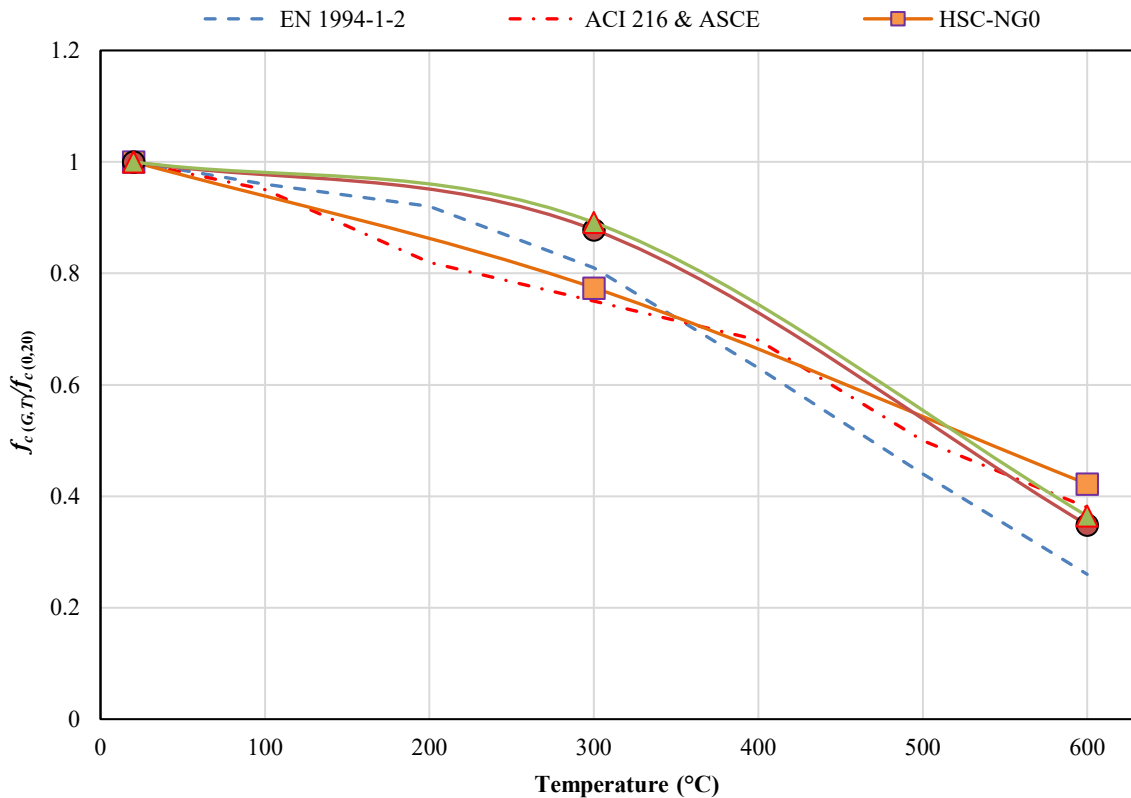
Fig. 11. Normalized compressive strength of concrete specimens in terms of temperature.

Using nonlinear regression analysis, Eq. 1 was developed to determine the compressive strength of specimens containing nylon granules exposed to elevated temperatures. In this equation, T represents the target temperature in degrees Celsius, T' is the temperature ratio, and G is the percentage of nylon granule replacement. Fig. 12 illustrates the trend of changes in normalized compressive strength concerning these parameters.

$$\frac{f_{c(G,T)}}{f_{c(0,20)}} = \left(-0.497T'^2 - 0.769T' + 1\right) + \left(-0.0591T'^2 + 0.0469T' - 0.0151\right)G$$
$$T' = \frac{T-20}{1000}$$

(1)
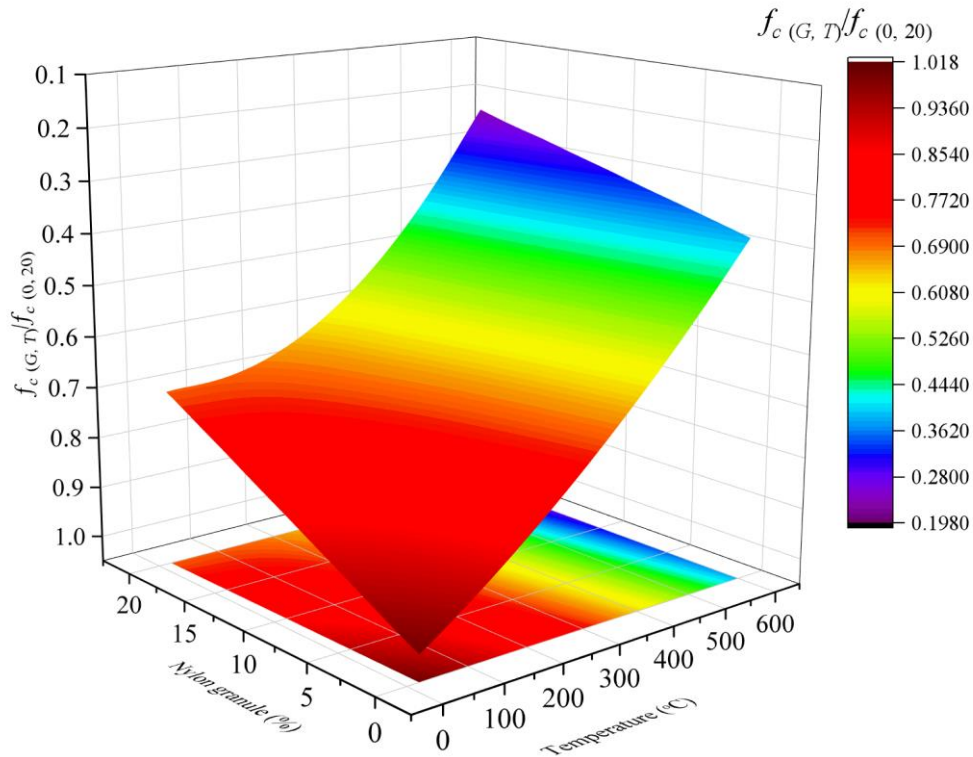
Fig. 12. Normalized compressive strength contour based on Eq. 1.

Based on the developed equation and the experimental data, several statistical performance indicators were used to evaluate the equation's accuracy. These indicators include the coefficient of correlation (R), coefficient of determination (R²), mean squared error (MSE), root mean squared error (RMSE), mean absolute error (MAE), and coefficient of variation (CV). The equations for these statistical performance indicators are presented in Eqs. 2 to 6.

$$R = \frac{\sum_{i=1}^{n}(m_i - \bar{m})(t_i - \bar{t})}{\sqrt{\sum_{i=1}^{n}(m_i - \bar{m})^2 \sum_{i=1}^{n}(t_i - \bar{t})^2}}$$

(2)

$$R^2 = \frac{\sum_{i=1}^{n}(m_i - \bar{m})^2}{\sum_{i=1}^{n}(t_i - \bar{t})^2}$$

(3)

$$MSE = \frac{\sum_{i=1}^{n}(m_i - t_i)^2}{n}$$

(4)

$$RMSE = \sqrt{\frac{\sum_{i=1}^{n}(m_i - t_i)^2}{n}}$$

(5)

$$MAE = \frac{\sum_{i=1}^{n}|m_i - t_i|}{n}$$

(6)

In these equations, n represents the number of input specimens used; m_i and t_i are the predicted and experimental values for the ith specimen, respectively. Additionally, $\bar{m}$ and $\bar{t}$ represent the mean of the predicted results and the mean of the experimental values, respectively. Table 7 summarizes the statistical performance indicators of Eq. 1 compared to the experimental results. According to the performance indicators listed in Table 7, the proposed Eq. 1 has successfully predicted the normalized compressive strength of the specimens with suitable accuracy.

Table 7. Statistical performance indicators results of Eq. 1.

R	R²	MAE	MSE	RMSE	Mean*	CV*(%)
0.997	0.995	0.0122	0.000309	0.0176	0.999	2.715

* Calculated for the predicted to experimental results ratio

Fig. 13 is presented to better understand the proposed relationship and compare it with the experimental data from this study as well as other studies in the literature (on concrete specimens containing recycled aggregates). The proposed relationship provides a relatively accurate estimation of the experimental results from other researchers [4, 52, 53].
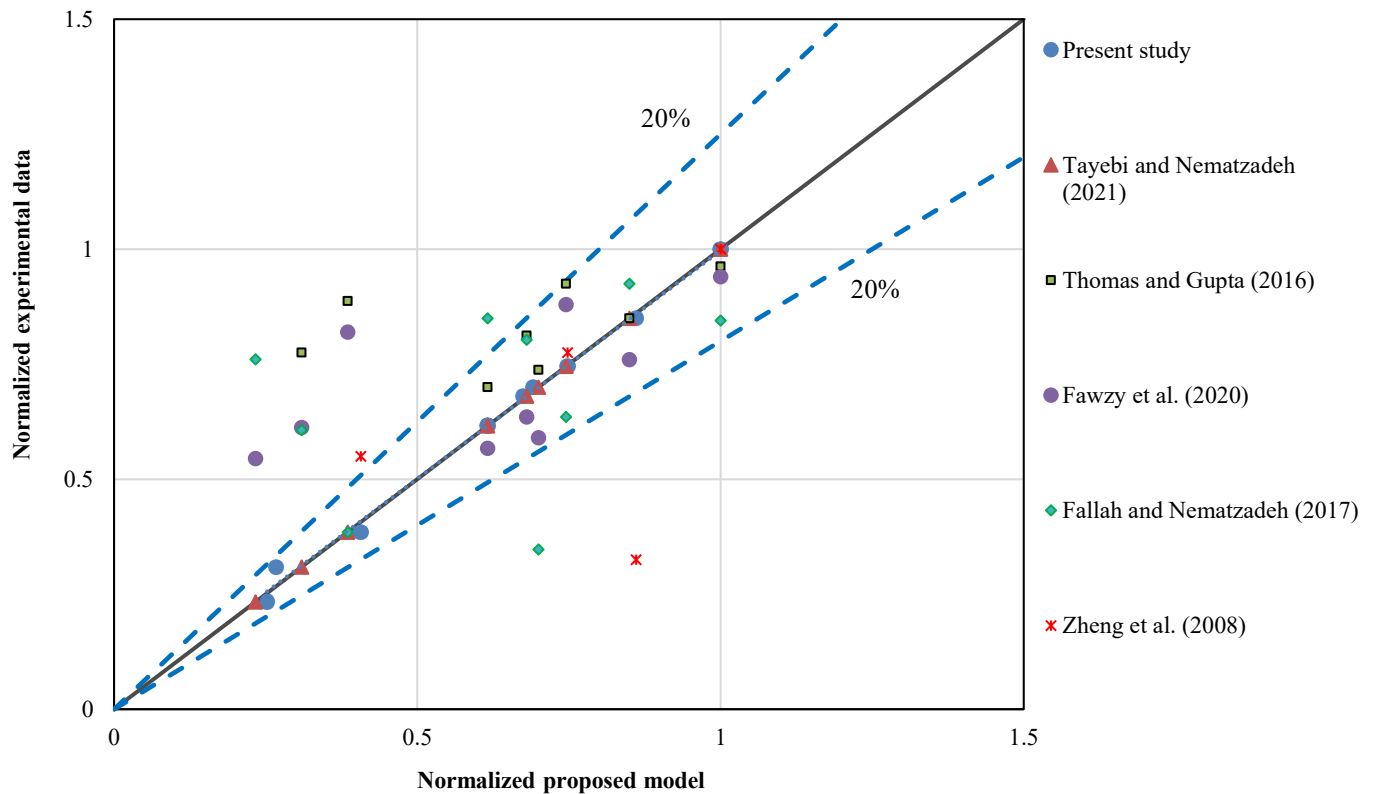

Fig. 13. Comparison of experimental data reported by different researchers with the equation proposed for compressive strength.

4.3. Splitting tensile strength

Splitting tensile strength is one of the most important mechanical properties of concrete, indicating the material's ability to resist indirect tensile forces. The results of the splitting tensile strength tests for all HSC cylindrical specimens containing NGs exposed to elevated temperatures are shown in Fig. 14 and Table 6. According to Table 6, the splitting tensile strength of the HSC specimens containing NG before and after exposure to elevated temperatures ranged from approximately 2 to 6 MPa. Similar to the compressive strength behavior, increasing both the exposure temperature and the nylon granule replacement percentage reduced the splitting tensile strength.

At room temperature, the splitting tensile strength of the HSC-NG10 and HSC-NG20 specimens decreased by 19.7 and 24.6%, respectively, compared to the reference specimen (without nylon granules). One reason for this reduction, similar to the compressive strength drop, is poor bonding between the nylon aggregates and the cement paste. Micro-cracks tend to form at the interface between the nylon granules and the paste, which accelerates the failure of the concrete. For nylon granules to contribute positively to splitting tensile strength, the bonding force between the granules and cement paste must exceed the force required to tear them, which is not the case in practice. Additionally, unlike natural fine aggregates, nylon granules have very smooth and non-porous surfaces, which interferes with aggregate interlocking and ultimately reduces both compressive and splitting tensile strength.

Upon exposure to 300°C, all specimens exhibited reduced splitting tensile strength. Specifically, the HSC-NG0, HSC-NG10, and HSC-NG20 specimens experienced decreases of 18, 8.2, and 8.7%, respectively. This reduction can be attributed to the formation of surface microcracks, internal stresses, and the chemical decomposition of the C-S-H gel at elevated temperatures. At 600°C, the strength loss peaked. The reductions in splitting tensile strength for the HSC-NG0, HSC-NG10, and HSC-NG20 specimens were 65.6, 59.2, and 65.2%, respectively, compared to their counterparts at 20°C. Notably, the 10% NG replacement specimens showed less tensile strength reduction compared to the other groups, suggesting some relative resilience under thermal exposure.

The normalized splitting tensile strength is defined as the ratio of the splitting tensile strength of a specimen exposed to a target temperature ($f_{t(G,T)}$) to the splitting tensile strength of the specimen at 20 °C ($f_{t(0,20)}$). Fig. 15 shows the values of normalized splitting tensile strength as a function of temperature based on EN 1994-1-2 [31]. This figure generally indicates that these codes provide reasonably accurate estimates of the tested specimens' normalized splitting tensile strength values. Furthermore, it appears that the presented experimental results closely align with the relationships proposed in the regulations.
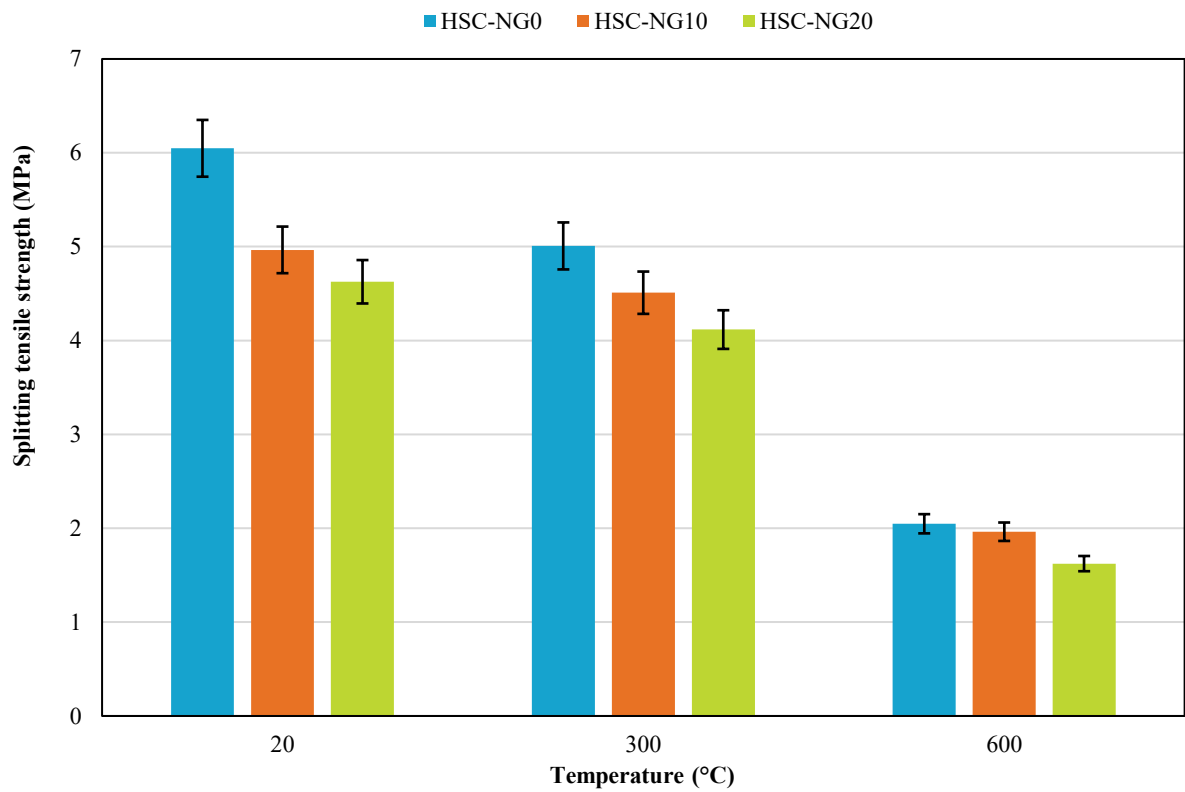
**Fig. 14. Splitting tensile strength of specimens before and after exposure to elevated temperatures.**
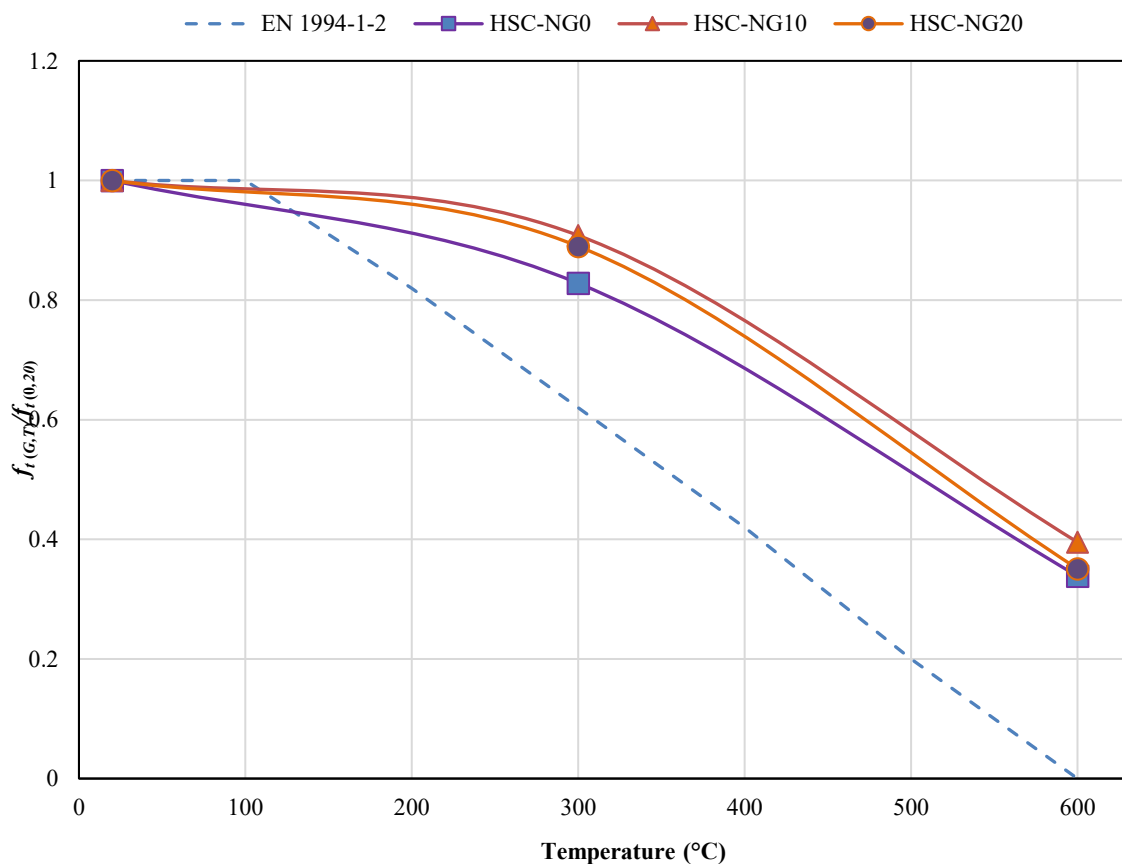
Fig. 15. Normalized splitting tensile strength of concrete specimens in terms of temperature.

Using nonlinear regression analysis, Eq. 7 was developed to determine the splitting tensile strength of specimens containing nylon granules exposed to elevated temperatures. In this equation, T represents the target temperature in degrees Celsius, T' is the temperature ratio, and G is the percentage of nylon granule replacement. Fig. 16 illustrates the trend of normalized splitting tensile

strength changes concerning these parameters.

$$\frac{f_{t(G,T)}}{f_{t(0,20)}} = (1 - 0.0657T' - 0.0136G - 1.834T'^2 + 0.0000321G^2 + 0.0165T'G) \tag{7}$$
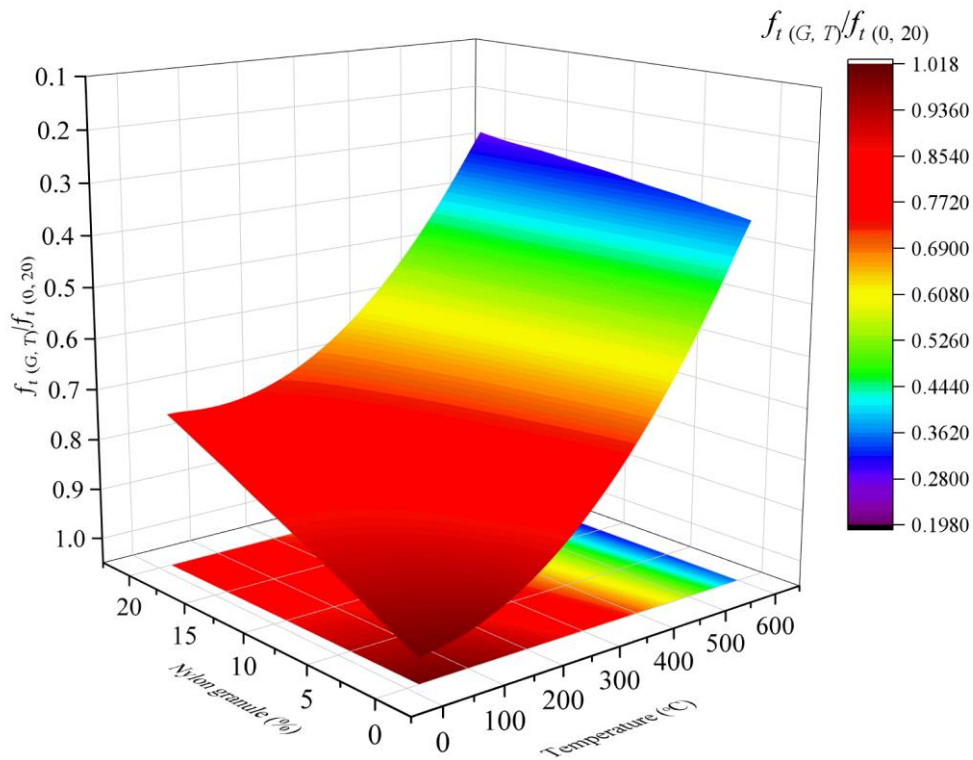
Fig. 16. Normalized initial modulus of elasticity contour based on Eq. 7.

Table 8 summarizes the statistical performance indicators of Eq. 7 compared to the experimental results. According to the performance indicators listed in Table 8, the proposed Eq. 7 has successfully predicted the normalized splitting tensile strength of the specimens with suitable accuracy. Fig. 17 is presented to better understand the proposed relationship and compare it with the experimental data from this study as well as other studies in the literature (on concrete specimens containing recycled aggregates). The proposed relationship provides a relatively accurate estimation of the experimental results from other researchers [7, 25, 54, 55].

Table 8. Statistical performance indicators results of Eq. 7.

R	R²	MAE	MSE	RMSE	Mean*	CV*(%)
0.997	0.994	0.0143	0.000371	0.0192	0.996	2.567

* Calculated for the predicted to experimental results ratio

4.4. Modulus of elasticity

The elastic modulus is a critical mechanical property of concrete that reflects its stiffness against elastic deformations under loading. In simpler terms, this parameter indicates the extent to which concrete deforms under a given stress. The elastic modulus is especially important in designing and analyzing structures where deformation and displacement are significant concerns. The values of the initial elastic modulus (tangent elastic modulus) for all concrete specimens are presented in Table 6 and Fig. 18. Additionally, the results for the secant modulus are shown in Table 6 and Fig. 19. The results reveal that increasing the replacement percentage of NG with natural fine aggregates reduces both the initial and secant elastic moduli across all target temperatures. It should also be noted that the reduction rate in elastic modulus decreases with increasing exposure temperature for all specimens. This reduction is mainly due to the weaker physical structure of nylon granules, especially at elevated temperatures, resulting in lower resistance to deformation compared to natural fine aggregates [7]. The elastic modulus of concrete specimens is significantly influenced by the size, shape, and type of aggregates used [56]. After exposure to 300°C, the initial elastic modulus of HSC-NG0, HSC-NG10, and HSC-NG20 specimens decreased by 6.9, 2.8, and 7.3%, respectively, compared to their corresponding values at 20°C.

Similarly, the secant modulus decreased by 11.2, 6.9, and 11.2%, respectively. The main reasons for these reductions are similar to those observed in the compressive and splitting tensile strength declines. According to the results, at 300°C, the highest reduction in both the initial and secant modulus occurred in specimens with 20% NG replacement, while the lowest reduction was observed in specimens with 10% NG replacement. The temperature of 300°C is close to the melting point of the nylon granules, leading to

weakened cohesion between particles and other concrete components, ultimately reducing deformation resistance [7, 57]. At 600°C, the initial elastic modulus of HSC-NG0, HSC-NG10, and HSC-NG20 specimens dropped by 74.8, 75.8, and 76.6%, respectively, compared to their values at 20°C. The secant modulus decreased by 76.3, 75.7, and 75%, respectively. Based on the results, at 600°C, the highest reduction in initial modulus was observed in the specimens with 20% NG replacement and the lowest in the control specimens without NG. Conversely, for the secant modulus, the greatest reduction occurred in the reference specimens, while the least reduction was seen in specimens with 20% NG replacement.
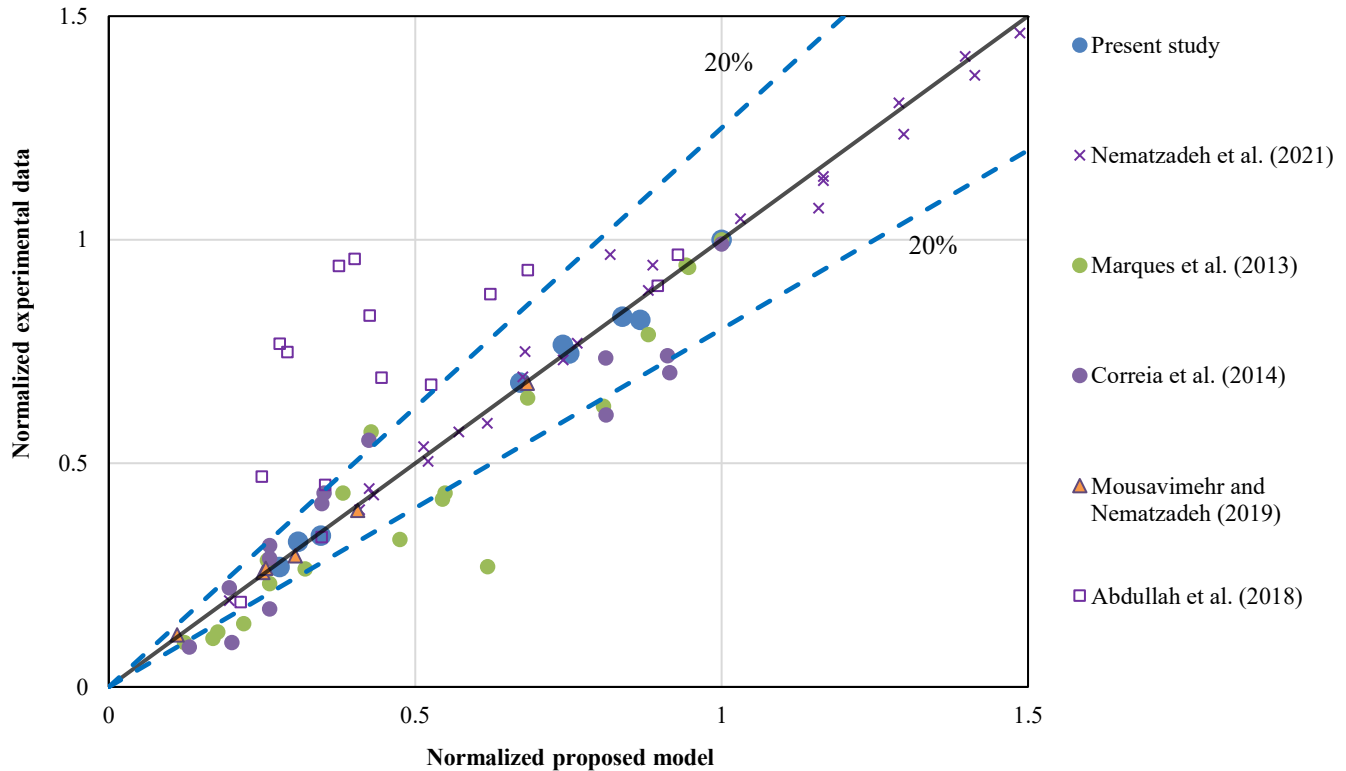
Fig. 17. Comparison of experimental data reported by different researchers with the equation proposed for splitting tensile strength.

These trends can be attributed to the decomposition of CH and the degradation of C-S-H gel, which increase the porosity of the cement paste and promote microcracking in the ITZ, ultimately reducing resistance to deformation [57]. Furthermore, heat exposure beyond the melting point of nylon granules and the loss of approximately 90% of their mass leads to void formation within the concrete, further decreasing both the initial and secant elastic moduli. The normalized initial modulus of elasticity is defined as the ratio of the initial modulus of elasticity of a specimen exposed to a target temperature ($E_{i(G,T)}$) to the initial modulus of elasticity of the specimen at 20 °C ($E_{i(0,20)}$).

The values of the normalized initial modulus of elasticity as a function of temperature, based on ASCE [30] and CEB-FIP [33], are shown in Fig. 20. Additionally, the normalized secant modulus of elasticity is defined as the ratio of the secant modulus of elasticity of a specimen exposed to a target temperature ($E_{s(G,T)}$) to the secant modulus of elasticity of the specimen at 20 °C ($E_{s(0,20)}$). The values of normalized secant modulus of elasticity as a function of temperature, based on ACI 216 [29], ASCE [30], and, EN 1994-1-2 [31] are shown in Fig. 21. These figures generally indicate that these codes provide reasonably accurate estimates of the initial and second modulus of elasticity values for the tested specimens. Furthermore, it appears that the presented experimental results closely align with the relationships proposed in the regulations.

Using nonlinear regression analysis, Eq. 8 was developed to determine the initial modulus of elasticity of specimens containing nylon granules exposed to elevated temperatures. In this equation, T represents the target temperature in degrees Celsius, T' is the temperature ratio, and G is the percentage of nylon granule replacement. Fig. 22 is presented to better illustrate the trend of changes in the normalized initial modulus of elasticity concerning these parameters.

$$\frac{E_{i(G,T)}}{E_{i(0,20)}} = (-3.506T'^2 + 0.732T' + 1) + (0.0209T'^2 - 0.003T' - 0.0078)G \tag{8}$$

Table 9 summarizes the statistical performance indicators of Eq. 8 compared to the experimental results. According to the performance indicators listed in Table 9, the proposed Eq. 8 has successfully predicted the normalized initial modulus of elasticity of the specimens with suitable accuracy.
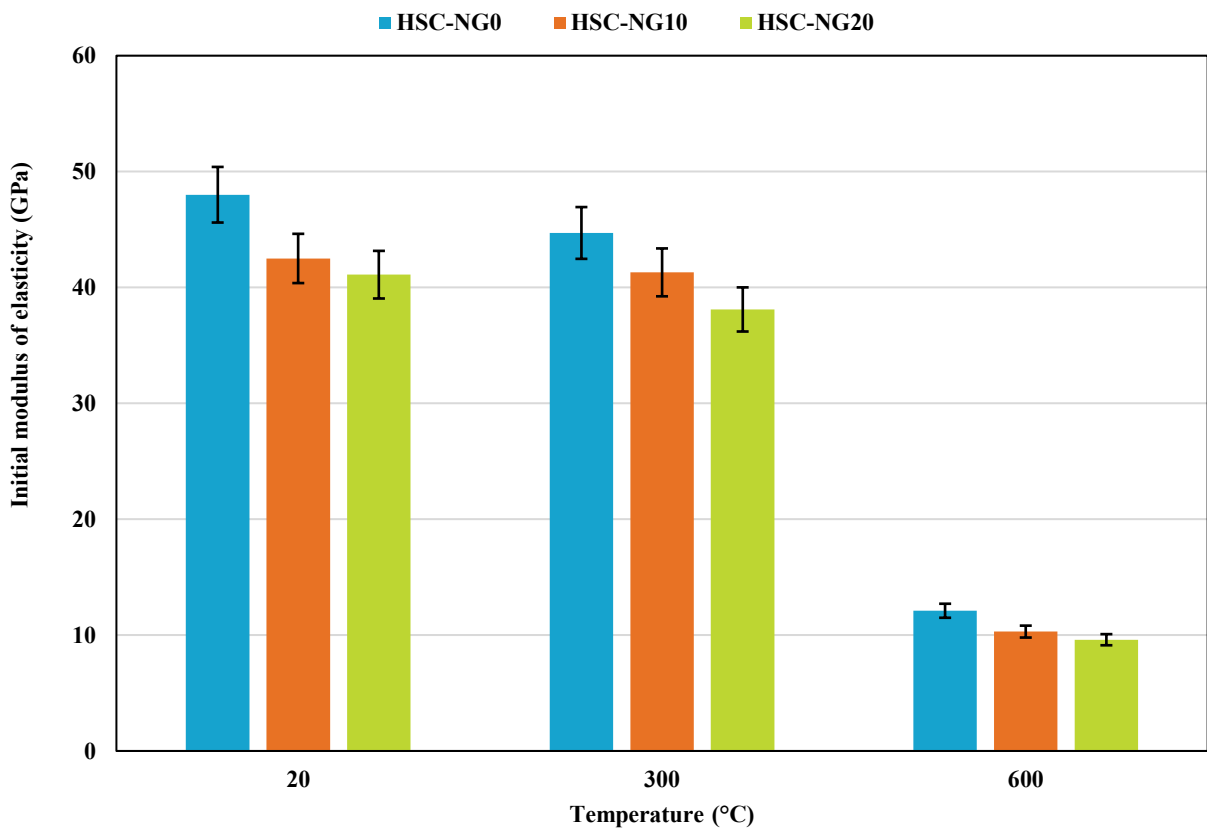
**Fig. 18. Initial modulus of elasticity of concrete specimens before and after exposure to elevated temperatures.**
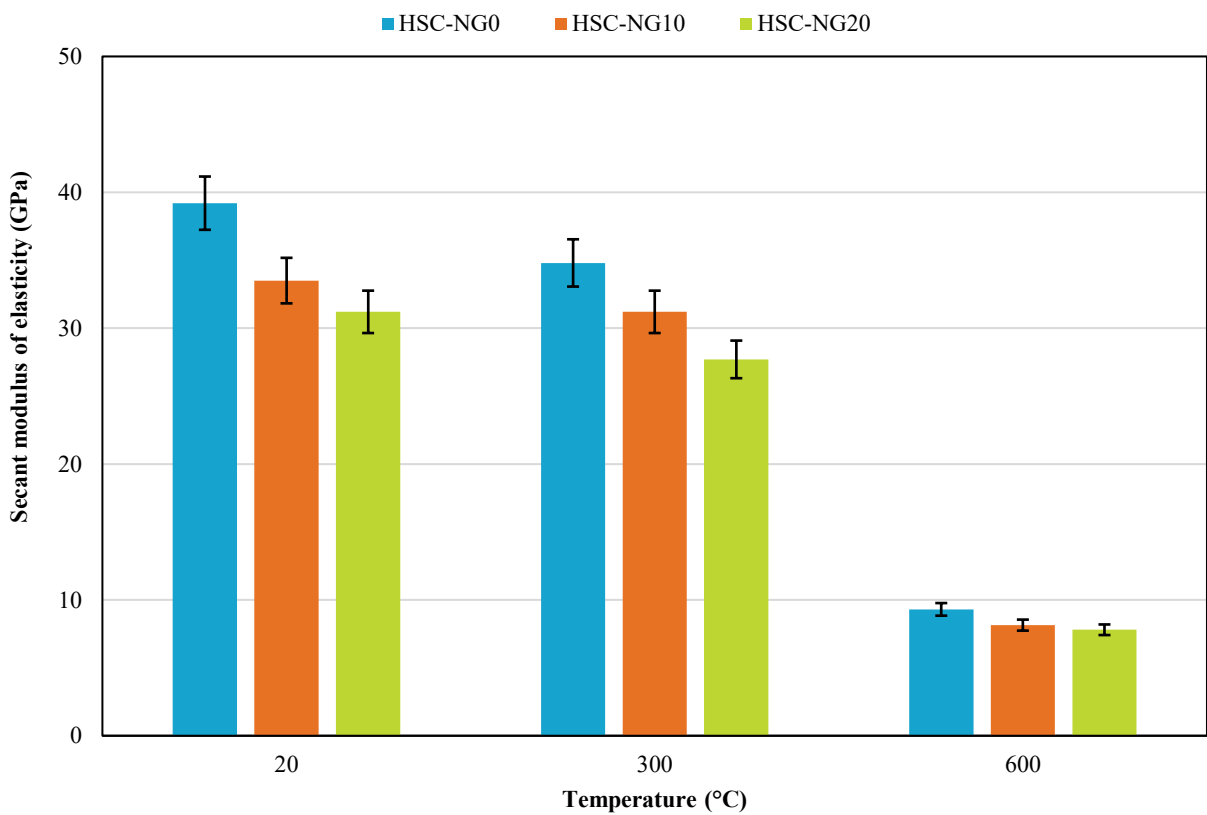
Fig. 19. Secant modulus of elasticity of concrete specimens before and after exposure to elevated temperatures.
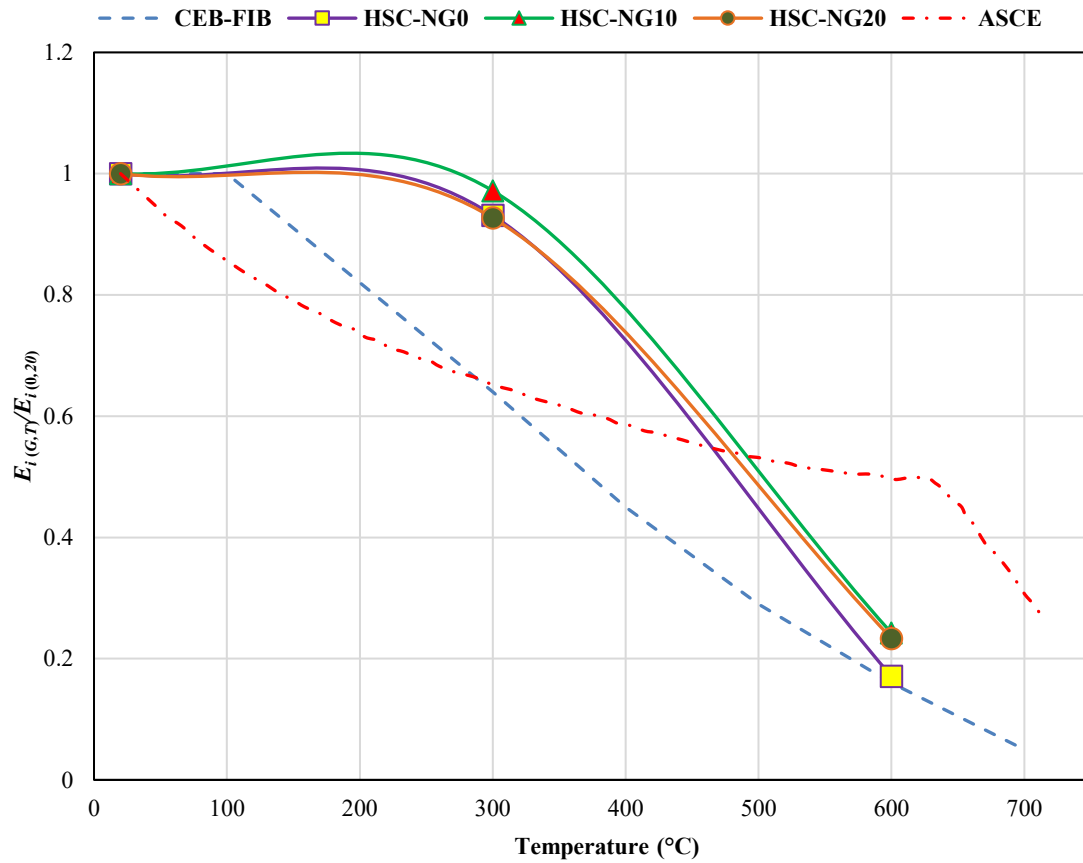
Fig. 20 Normalized initial modulus of elasticity of concrete specimens in terms of temperature.
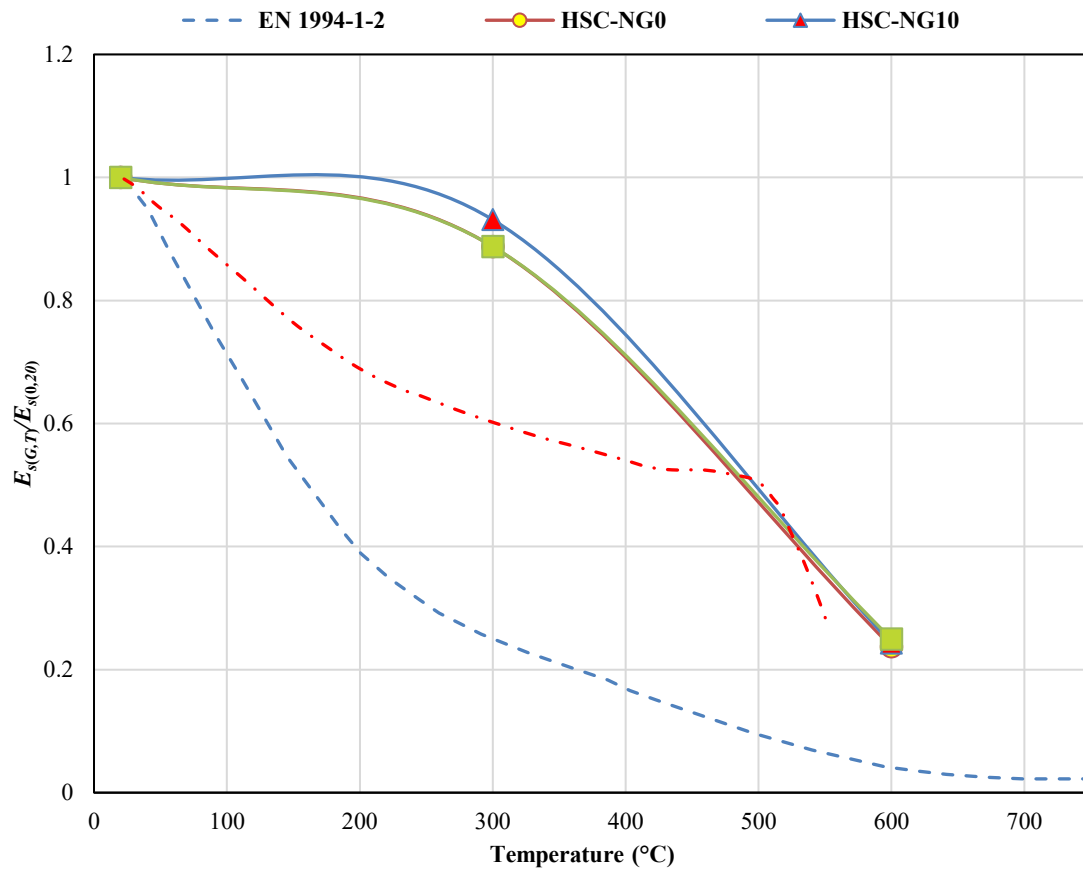

**Fig. 21. Normalized secant modulus of elasticity of concrete specimens in terms of temperature.**
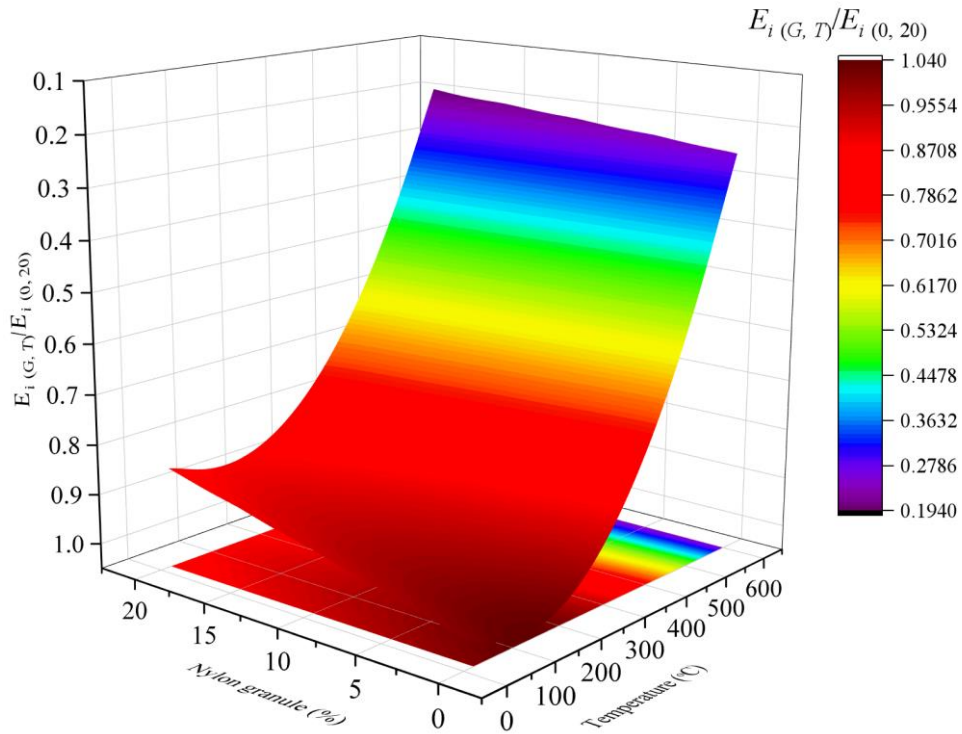
Fig. 22. Normalized initial modulus of elasticity contour based on Eq. 8.

Table 9. Statistical performance indicators results of Eq. 8.

R	R²	MAE	MSE	RMSE	Mean*	CV*(%)
0.999	0.998	0.00794	0.000179	0.0134	0.999	2.211

* Calculated for the predicted to experimental results ratio

Fig. 23 is presented to better understand the proposed relationship and compare it with the experimental data from this study as well as other studies in the literature (on concrete specimens containing recycled aggregates). The proposed relationship provides a relatively accurate estimation of the experimental results from other researchers [4, 22, 52, 53].
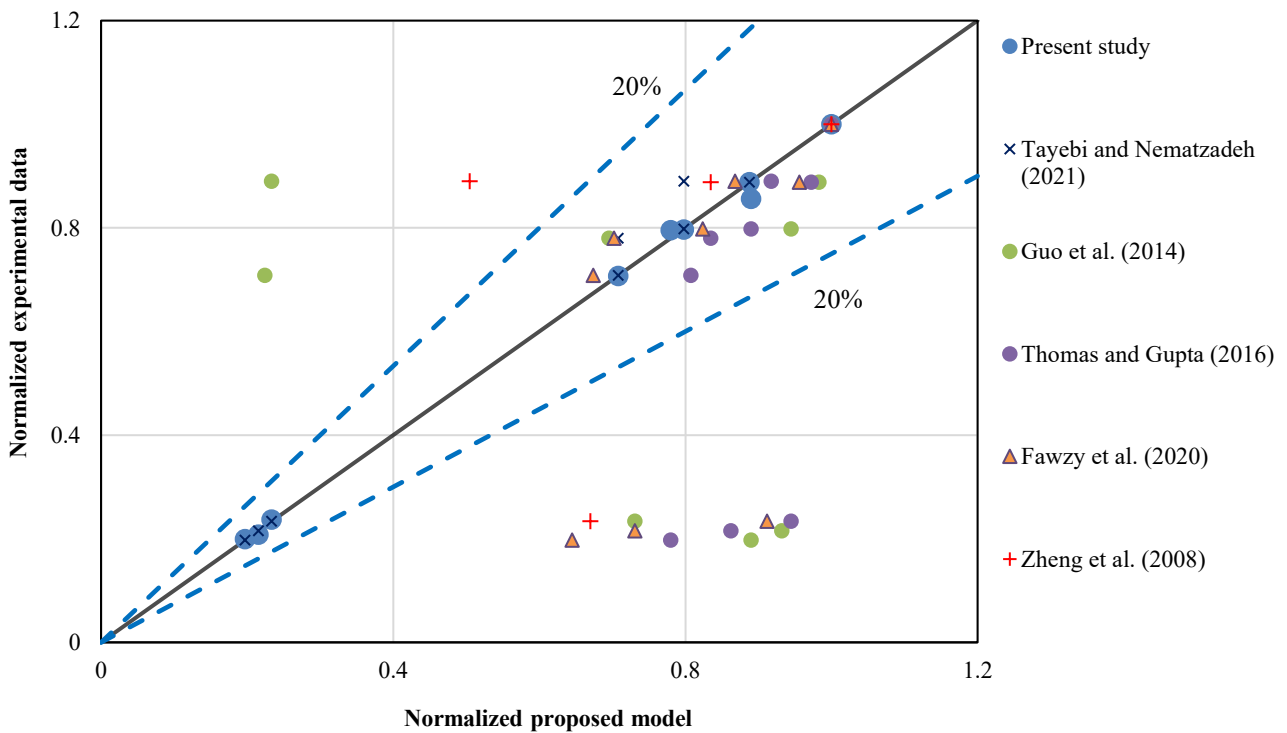
Fig. 23. Comparison of experimental data reported by different researchers with the equation proposed for the initial modulus of elasticity.

Using nonlinear regression analysis, Eq. 9 was developed to determine the secant modulus of elasticity of specimens containing nylon granules exposed to elevated temperatures. In this equation, T represents the target temperature in degrees Celsius, T' is the temperature ratio, and G is the percentage of nylon granule replacement. Fig. 24 is presented to better illustrate the trend of changes in the normalized secant modulus of elasticity concerning these parameters.

$$\frac{E_{s(G,T)}}{E_{s(0,20)}} = (-3.077T'^2 + 0.469T' + 1) + (0.0279T'^2 - 0.00067T' - 0.011)G \tag{9}$$
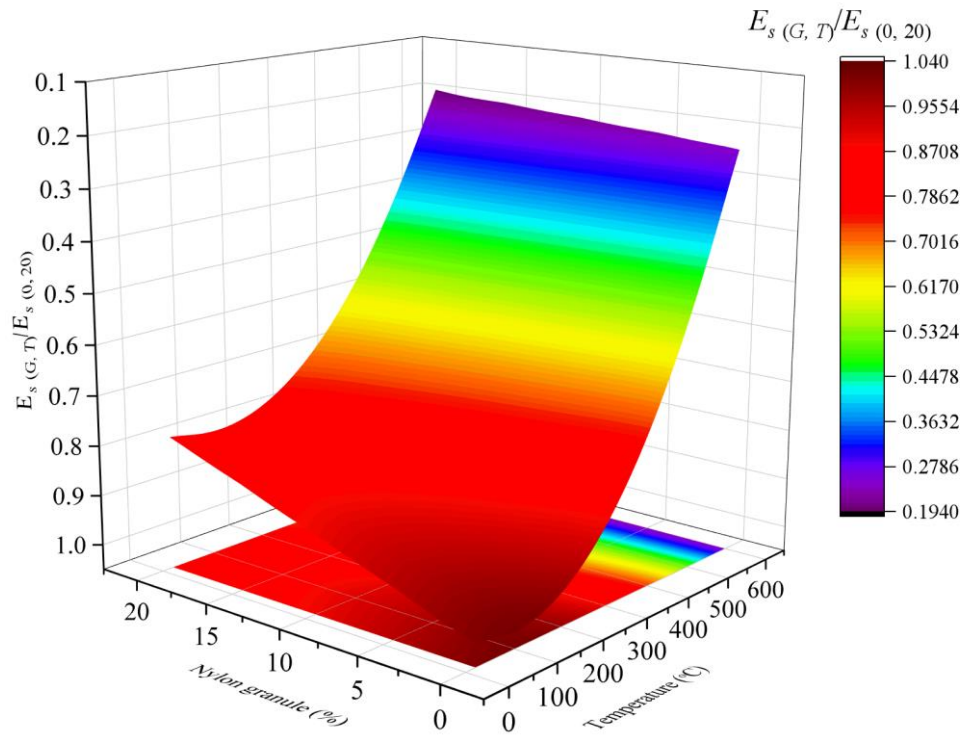
Fig. 24. Normalized secant modulus of elasticity contour based on Eq. 9.

Table 10 summarizes the statistical performance indicators of Eq. 9 compared to the experimental results. According to the performance indicators listed in Table 10, the proposed Eq. 9 has successfully predicted the specimens' normalized secant modulus of elasticity with suitable accuracy.

Table 10. Statistical performance indicators results of Eq. 9.

R	R²	MAE	MSE	RMSE	Mean*	CV*(%)
0.999	0.998	0.00814	0.000181	0.0134	0.995	2.356

* Calculated for the predicted to experimental results ratio

Fig. 25 is presented to better understand the proposed relationship and compare it with the experimental data from this study as well as other studies in the literature (on concrete specimens containing recycled aggregates). The proposed relationship provides a relatively accurate estimation of the experimental results from other researchers [12, 54, 58, 59].

4.5. Strain at peak stress

Table 11 and Fig. 26 present the peak strain (strain at peak stress) values for all specimens. According to the results, the peak strain ranged between 0.002 mm/mm and 0.0056 mm/mm. Notably, the minimum and maximum peak strain values were observed for the HSC-NG20 specimen at room temperature and the HSC-NG0 specimen at 600°C, respectively. At ambient temperature, the HSC-NG10 sample exhibited the highest peak strain. Moreover, the results indicate that the peak strain significantly changed after exposure to 600°C, which is consistent with findings from Akbarzadeh Bengar et al. [60]. Upon heating the specimens to 300°C, the peak strain ranged between 0.0022 mm/mm and 0.0035 mm/mm, which is comparable to the range observed at room temperature. However, after exposure to 600°C, all specimens showed a substantial increase in peak strain. This trend is attributed to the concrete softening due to heat and the loss of cohesion between the cement paste and aggregates at high temperatures [48]. Based on the data in Table 10, it was found that for most specimens except HSC-NG10 at room temperature and 300°C, an increase in the nylon granule replacement ratio reduced peak strain compared to the control specimens without nylon granules. Additionally, peak strain increased with rising exposure temperatures. Specifically, after exposure to 600°C, the peak strain increased by 166.7, 46.9, and 90% for the HSC-NG0, HSC-NG10, and HSC-NG20 specimens, respectively. The normalized strain at peak stress is defined as the ratio of the strain at peak stress of a specimen exposed to a target temperature ($\varepsilon_{c(G,T)}$) to the strain at peak stress of the specimen at 20 °C ($\varepsilon_{c(0,20)}$).
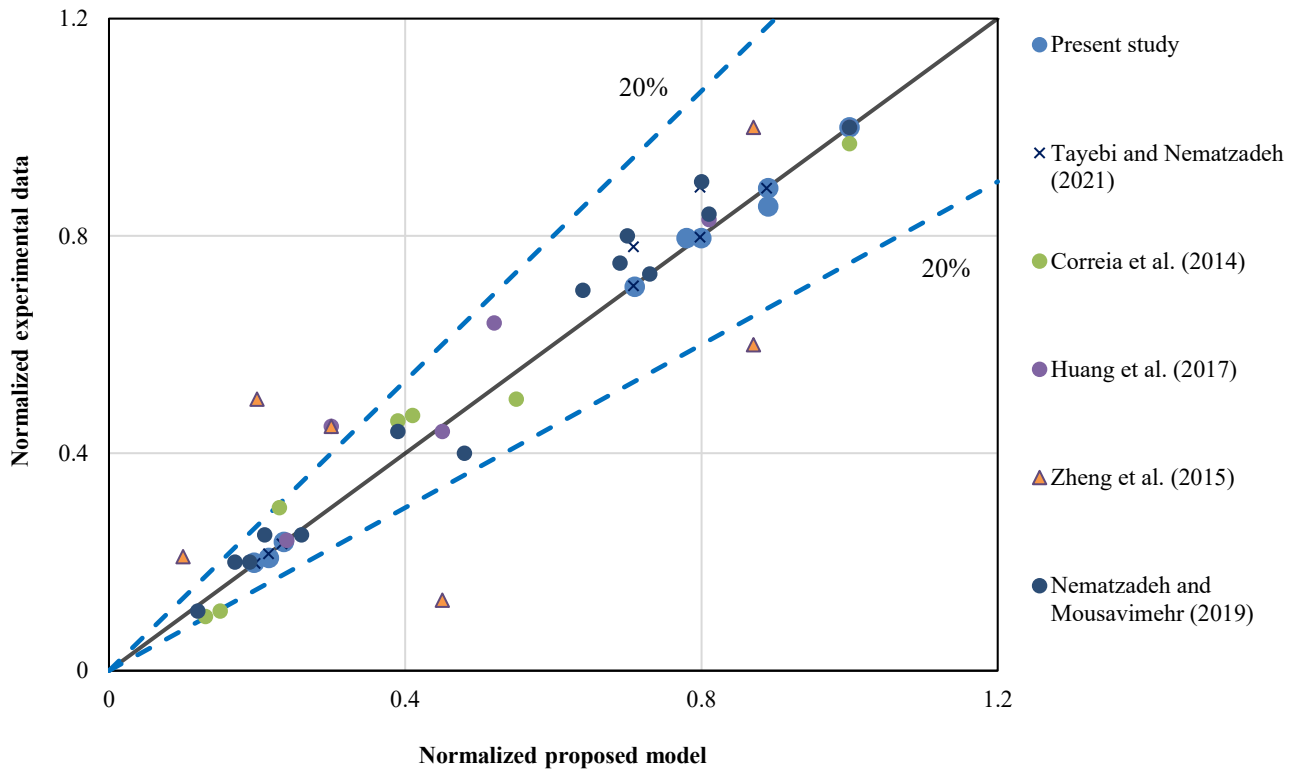
Fig. 25. Comparison of experimental data reported by different researchers with the equation proposed for the secant modulus of elasticity.

Table 11. Axial strain and toughness values of the specimens at elevated temperatures.

Specimen ID	Temperature (°C)	Strain at peak stress (mm/mm)	Ultimate strain (Residual strength of $0.3f'_c$)	Ultimate strain (Residual strength of $0.85f'_c$))	Toughness (J/m³)
	20	0.0021	0.0031	0.0027	0.089
HSC-NG0	300	0.0027	0.0037	0.0033	0.083
	600	0.0056	0.0081	0.0072	0.087
	20	0.0032 (+52.4%)	0.0062	0.0048	0.071
HSC-NG10	300	0.0035 (+29.6%)	0.0065	0.005	0.065
	600	0.0047 (-16.0%)	0.0067	0.0061	0.064
	20	0.002 (-4.8%)	0.0031	0.0031	0.069
HSC-NG20	300	0.0022 (-25.9%)	0.0033	0.0035	0.064
	600	0.0038 (-32.1%)	0.0055	0.0065	0.054

Fig. 27 shows the values of normalized strain at peak stress as a function of temperature based on EN 1994-1-2 [31]. This figure generally indicates that these codes provide reasonably accurate estimates of the normalized strain at peak stress values for the tested specimens. Furthermore, it appears that the presented experimental results closely align with the relationships proposed in the regulations.

Using nonlinear regression analysis, Eq. 10 was developed to determine the strain of specimens containing nylon granules exposed to elevated temperatures at peak stress. In this equation, T represents the target temperature in degrees Celsius, T' is the temperature ratio, and G is the percentage of nylon granule replacement. Fig. 28 is presented to better illustrate the trend of changes in the normalized strain at peak stress concerning these parameters.

$$\frac{\varepsilon_{c(G,T)}}{\varepsilon_{c(0,20)}} = (1 - 0.0855T' + 0.0735G + 4.621T'^2 - 0.00361G^2 - 0.0685T'G) \tag{10}$$

Table 11 summarizes the statistical performance indicators of Eq. 10 compared to the experimental results. According to the performance indicators listed in Table 11, the proposed Eq. 10 has successfully predicted the normalized strain at peak stress of the specimens with suitable accuracy.

Fig. 29 is presented to better understand the proposed relationship and compare it with the experimental data from this study as well as other studies in the literature (on concrete specimens containing recycled aggregates). The proposed relationship provides a relatively accurate estimation of the experimental results from other researchers [4, 52, 61].
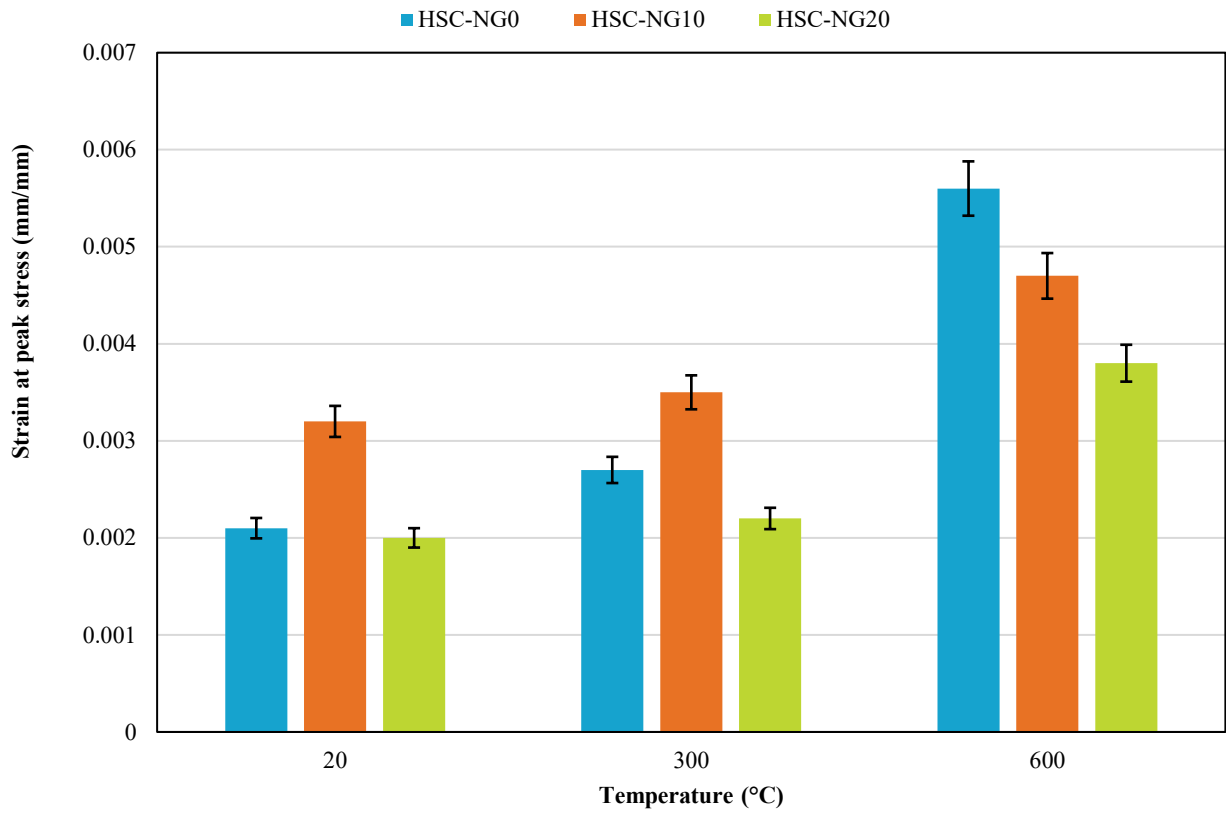
Fig. 26. Strain at peak stress of concrete specimens before and after exposure to elevated temperatures.
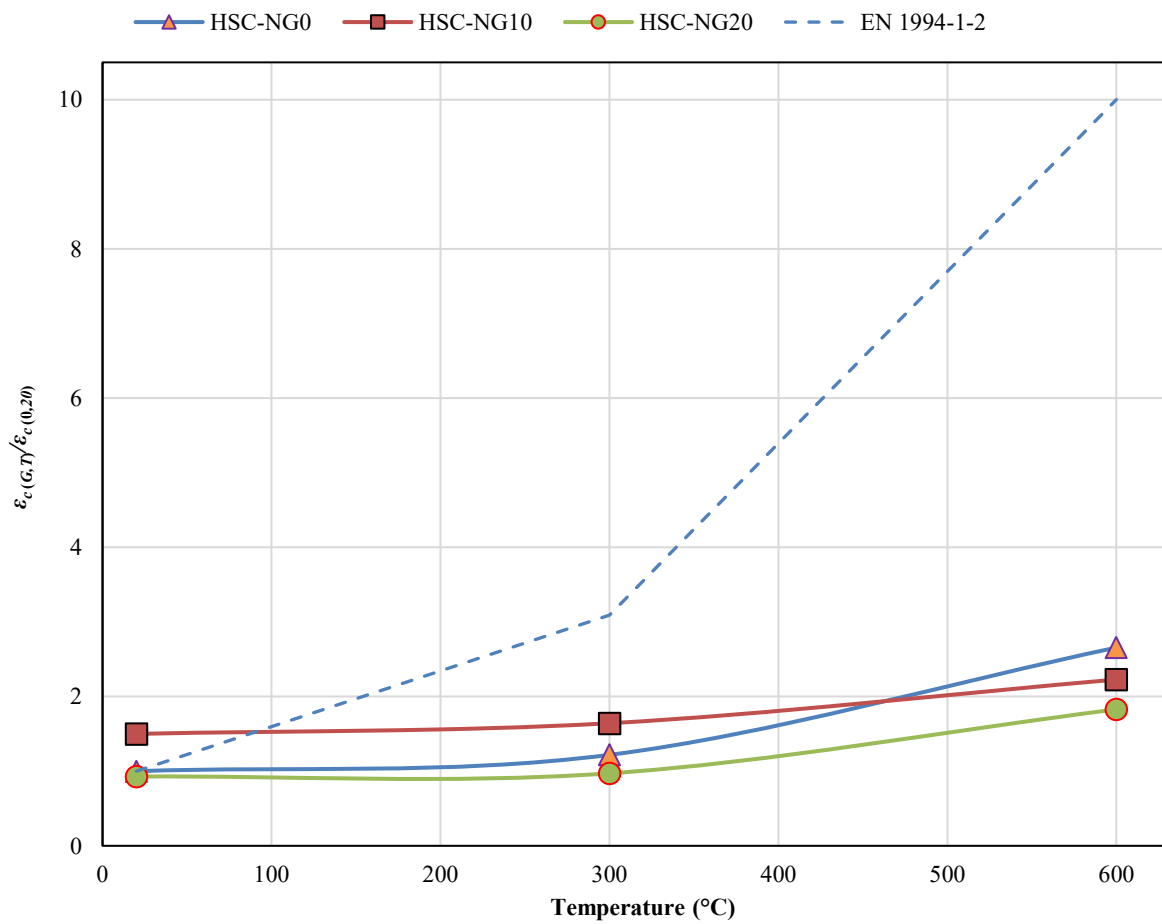

Fig. 27. Normalized strain at peak stress of concrete specimens in terms of temperature.
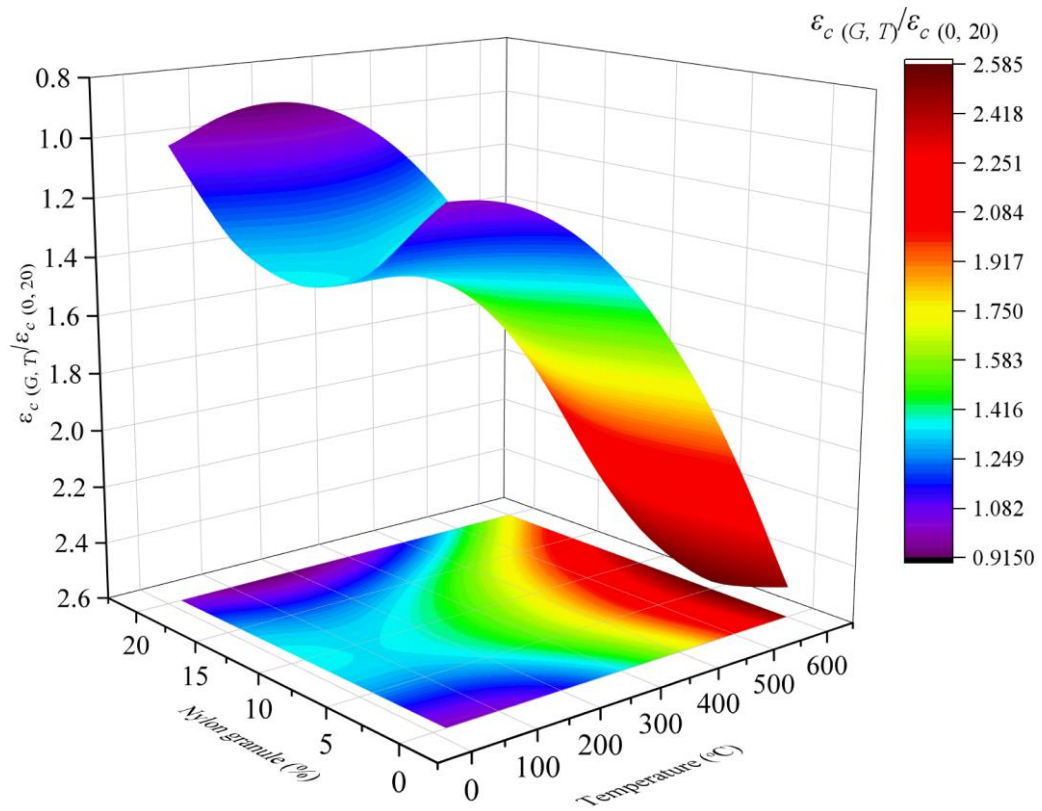
Fig. 28. Normalized strain at peak stress contour based on Eq. 10.

Table 11. Statistical performance indicators results of Eq. 10.

R	R²	MAE	MSE	RMSE	Mean*	CV*(%)
0.974	0.948	0.108	0.0167	0.129	1.008	2.972

* Calculated for the predicted to experimental results ratio
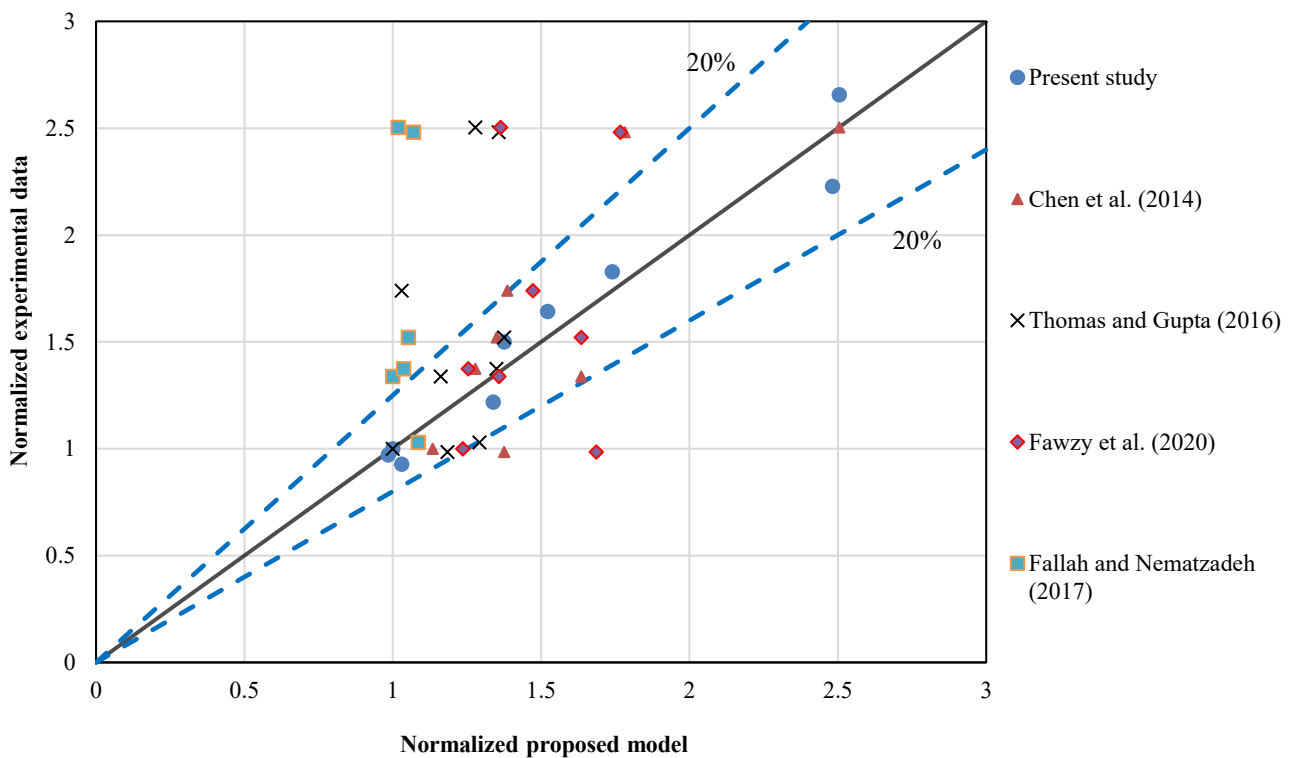
Fig. 29. Comparison of experimental data reported by different researchers with the equation proposed for the strain at peak stress.

4.6. Ultimate strain

To describe the post-peak stress-strain behavior of concrete, several criteria are typically employed to define the descending branch of the stress-strain curve. For example, Sheikh and Uzumeri [62] used the strain corresponding to a 70% drop in compressive strength (i.e., 30% residual compressive strength) as the ultimate strain, while Frangou et al. [63] considered the strain at a 15% strength drop (i.e., 85% residual compressive strength) as the ultimate strain. The corresponding values of ultimate strain based on these two criteria are presented in Figs. 30 and 31, respectively. Additionally, the exact values of the ultimate strain for the concrete specimens are provided in Table 10. According to the results presented in Figs. 30 and 31, at room temperature and 300°C, the highest ultimate strain was observed in the specimens with 10% NG replacement. However, it should also be noted that the maximum ultimate strain at 600°C occurred in the control specimens without NG. After exposure to 300°C, the ultimate strain in all specimens increased compared to those tested at room temperature. This increase is attributed to the softening and ductility of nylon granules near their decomposition temperature, CH dehydration, and the degradation of C-S-H gel. When exposed to 600°C, the decomposition of nylon granules, softening, and dehydration of cement paste further increased the ultimate strain. In the specimens containing NG, significant mass loss was observed at 600°C (see Fig. 9), which resulted in increased porosity. Nevertheless, this increased porosity facilitates the release of trapped gases within concrete voids, thereby reducing internal cracking and, in turn, enhancing the specimens' ultimate strain capacity.
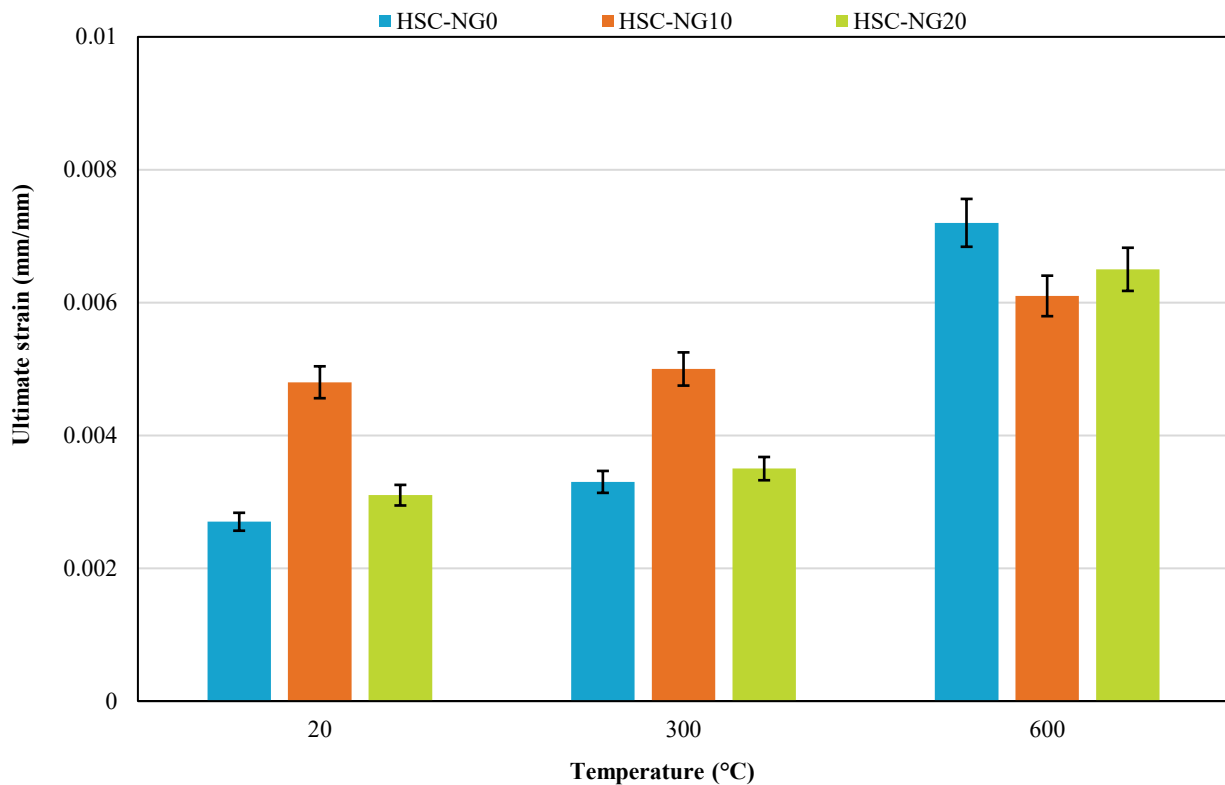

Fig. 30. Ultimate strain corresponding to a 15% reduction in compressive strength.

4.7. Toughness

The toughness of concrete specimens under axial compression is defined as the area under the stress-strain curve up to the peak stress point [64, 65]. The results related to the toughness of all HSC specimens containing NG are presented in Table 10 and Fig. 32. According to the results, the toughness of the reference specimens (without NG replacement) was greater than that of all NG-containing specimens at all tested temperatures. Furthermore, the toughness decreased at all temperature levels with an increase in NG replacement percentage. This reduction is attributed to reference specimens' higher compressive strength than those containing NG. Moreover, the peak strain values for all specimens were relatively close to each other, which resulted in a greater area under the stress-strain curve (i.e., higher toughness) for the control specimens. Additionally, the toughness of all concrete specimens decreased with increasing temperature. This nonlinear trend in toughness reduction with temperature is due to the simultaneous decrease in compressive strength and increase in peak strain with rising temperature, which have opposite effects on the resulting toughness.

4.8. Stress-strain behavior and proposed model

The axial compressive stress-strain curves for all specimens are plotted in separate groups in Fig. 33. These curves allow for the evaluation of changes in compressive strength, elastic modulus, peak strain, and toughness. Based on the stress-strain curves shown in Fig. 33, the ascending branch of NG-containing concrete specimens exhibits a more nonlinear behavior compared to reference specimens (without NG), particularly at 300 and 600°C. This behavior is attributed to the thermal degradation of NG particles at elevated temperatures and the formation of internal voids within the concrete matrix.
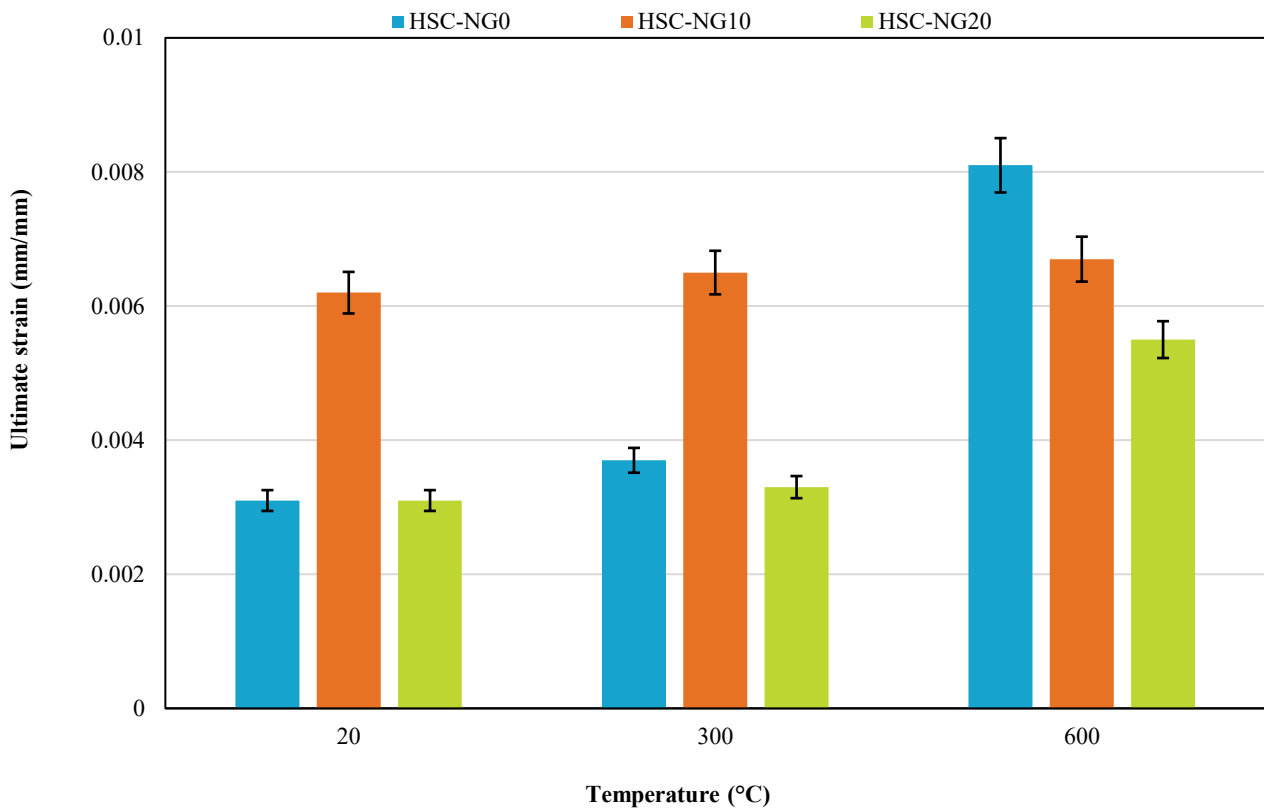
**Fig. 31. Ultimate strain corresponding to a 70% reduction in compressive strength.**
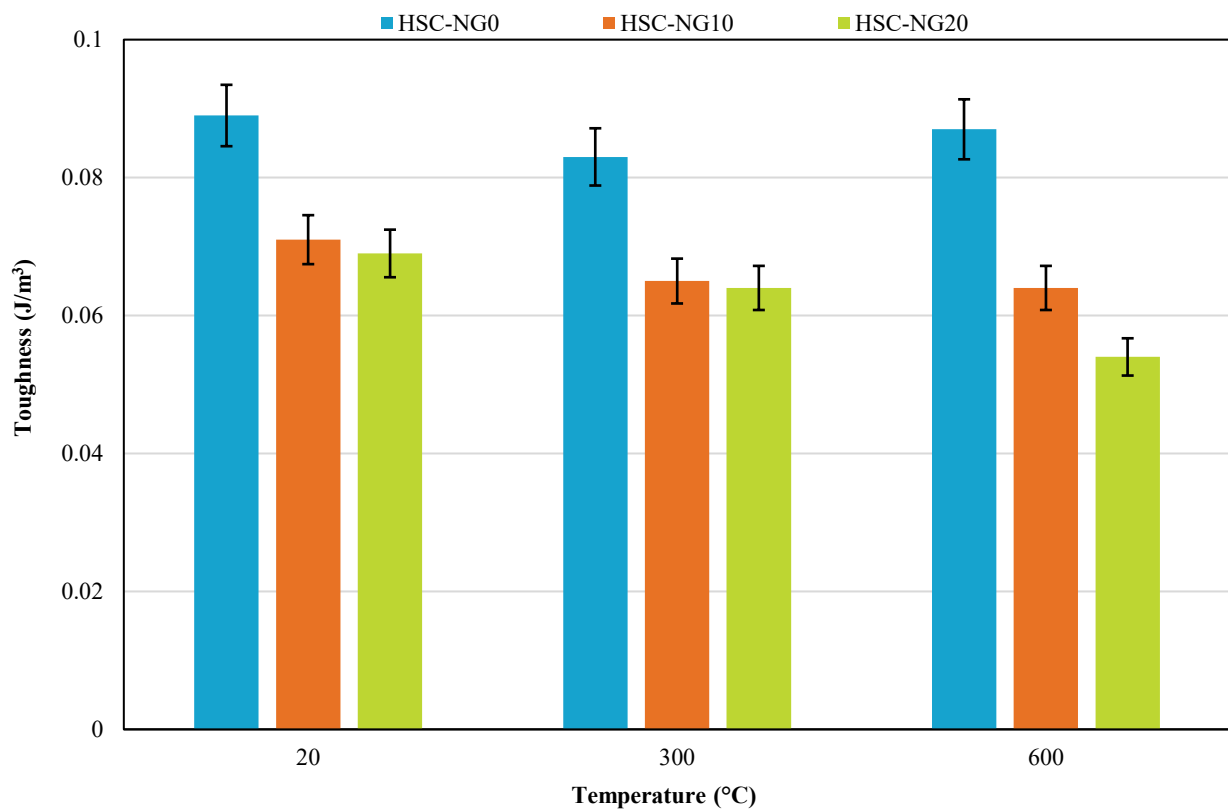
Fig. 32. Toughness of concrete specimens before and after exposure to elevated temperatures.

Additionally, as the exposure temperature increases, the overall shape of the stress-strain curve changes, with a reduction in the slope of both the ascending and descending branches. Notably, an increase in peak strain eventually accompanies the decrease in slope in the descending branch. This study predicted the stress-strain behavior of concrete specimens exposed to elevated temperatures based on the relationships provided in previous sections. To predict the stress-strain response of high-strength concrete specimens containing NG after thermal exposure, the model proposed by Nematzadeh et al. [66] was utilized. Given the noticeable difference in behavior between the pre-peak and post-peak regions, separate equations were employed for the ascending and

descending branches of the stress-strain curve. Specifically, Eqs. 11 and 12 were used to model the ascending branch of the stress–strain behavior.

$$f_c = f_{c(G,T)} \frac{m\left(\frac{\varepsilon}{\varepsilon_{c(G,T)}}\right)}{m\left(\frac{\varepsilon}{\varepsilon_{c(G,T)}}\right) - \left(\frac{\varepsilon}{\varepsilon_{c(G,T)}}\right)^{1/\ln m}} \quad 0 \le \left(\frac{\varepsilon}{\varepsilon_{c(G,T)}}\right) \le 1 \tag{11}$$

$$m = \frac{E_{i(G,T)}\varepsilon_{c(G,T)}}{f_{c(G,T)}} \tag{12}$$

where ε represents the axial strain of the concrete specimens at any moment, and $f_{c(G,T)}$, $\varepsilon_{c(G,T)}$, and $E_{i(G,T)}$ denote the axial compressive strength, strain at peak stress, and initial elastic modulus of the concrete specimens, respectively. These parameters were calculated based on Eqs. 1, 8, and 10. For the descending branch, Eq. 13 was employed.

$$f_c = f_{c(G,T)} \frac{\alpha\left(\frac{\varepsilon}{\varepsilon_{c(G,T)}}\right)}{(\alpha-1)\left(\frac{\varepsilon}{\varepsilon_{c(G,T)}}\right) + e^{\frac{\left[\left(\frac{\varepsilon}{\varepsilon_{c(G,T)}}\right)^n - 1\right]}{n}}} \tag{13}$$

where $\alpha = 1$ and $n = 0.2\left(f_{c(G,T)} + 20\right)^{-0.25}$ are parameters obtained through trial-and-error and by calibrating the proposed model with the experimental results. To validate the proposed stress-strain relationship, the experimental stress-strain behavior of HSC specimens containing NG exposed to temperatures ranging from 20 to 600°C was compared with the predictions of the proposed model, as illustrated in Fig. 33. According to Fig. 33, the proposed model accurately predicted the stress-strain behavior in all cases except for the HSC-NG10 specimen exposed to 20°C, where the model failed to provide a good fit with the experimental data.
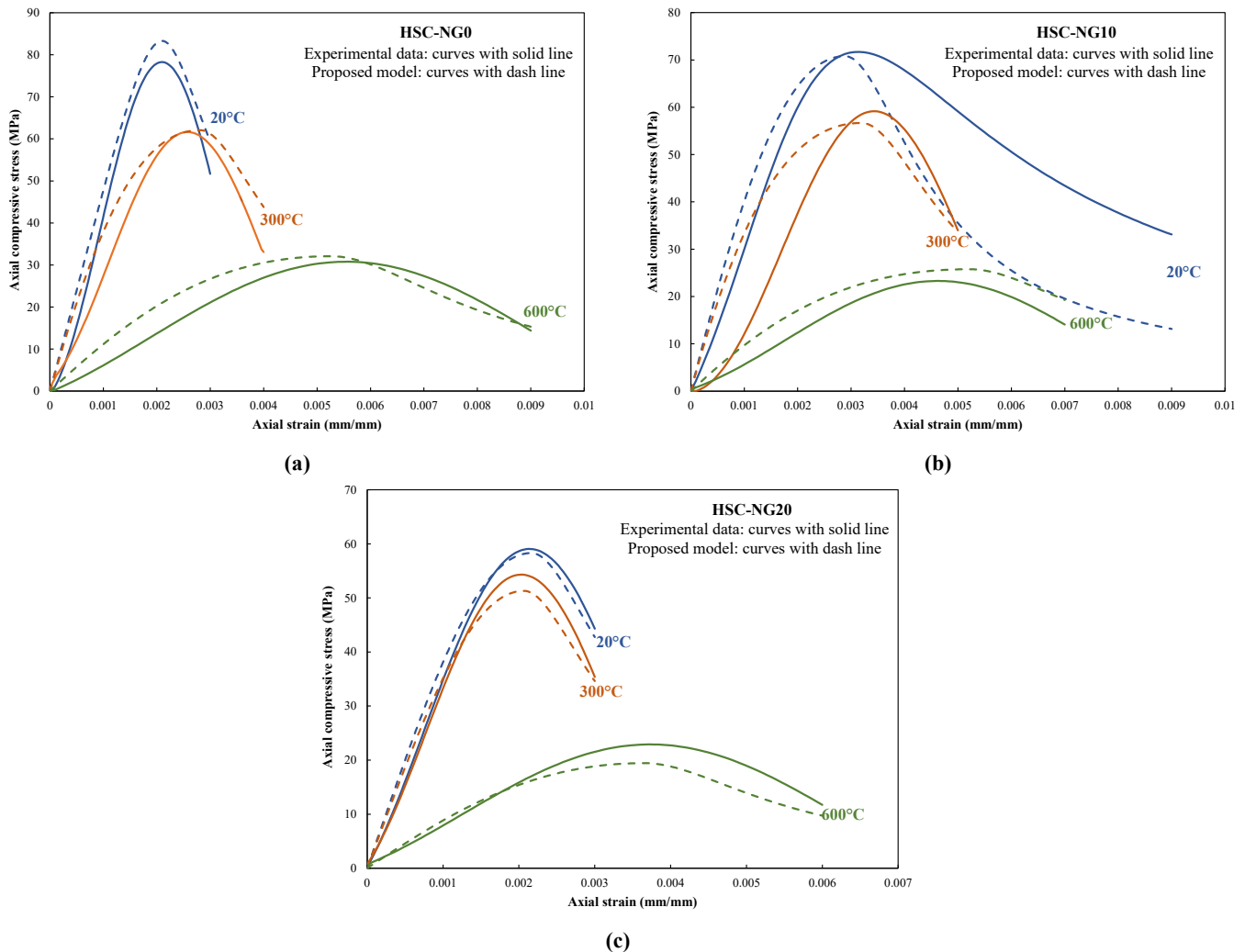

Fig. 33. Stress-strain curves obtained from the proposed model compared with experimental results of concrete specimens; (a) HSC-NG0, (b) HSC-NG10, and (c) HSC-NG20.

4.9. Visual observations and failure modes

The damage sustained by concrete due to fire is generally identifiable through visual inspection of its surface. Typical signs on concrete surfaces after fire exposure include color change, cracking, and spalling. This study examined the surfaces of concrete specimens exposed to high temperatures and subsequently removed from the electric furnace for such changes. The condition of

HSC specimens containing NG after exposure to different temperatures is shown in Fig. 34, while Fig. 35 displays the specimens with the highest NG replacement ratio after heating. Based on the images of the specimen surfaces, all specimens' color gradually changed from dark gray to light gray as the exposure temperature increased.

Specimen	20 °C	300 °C	600 °C
HSC-NG0®			
HSC-NG10			
HSC-NG20			

Fig. 34. Surface of HSC specimens containing NG after exposure to elevated temperatures.

HSC-NG20-20	HSC-NG20-300	HSC-NG20-600

Fig. 35. Top surface HSC specimens containing NG after exposure to elevated temperatures.

Additionally, after exposure to 300°C, surface cracks appeared on all specimens. When the temperature reached 600°C, the number and width of these cracks increased significantly (Figs. 30 and 32). These effects can be attributed to the evaporation of free and surface moisture, as well as the dehydration of chemically bound water in the C-S-H gel, which leads to internal stresses, microcracking, and color change [52]. In addition to cracking, the number of surface pores on the specimens increased significantly after exposure to high temperatures. In specimens containing NG granules, the increase in temperature and subsequent degradation of these particles led to a substantial rise in internal porosity, ultimately resulting in concrete porosity. Given the melting point of nylon granules, at around 300°C, they begin to soften and migrate toward the internal or surface pores of the concrete (see Figs. 34 and 36). As shown in Fig. 34, at 600°C, the NG particles are completely degraded. Specifically, in the HSC-NG10 specimen, the NG particles are entirely decomposed and evaporated through the cracks and pores formed on the surface after exposure to 600°C. Furthermore, in the HSC-NG20 specimen, due to the higher NG replacement ratio, some of the NG particles are fully degraded, while others are partially decomposed and evaporated, as illustrated in Fig. 31. Thus, at 300°C, nylon granules first enter their plastic phase and then exceed their decomposition point, eventually evaporating as harmful gases with unpleasant odor through surface cracks and pores as the temperature approaches 600°C. This leads to the removal of NG granules from the concrete matrix and the formation of voids. Overall, the nylon granules partially re-solidify after the thermal exposure and cooling process. As shown in Fig. 30, they remain on the surface of the concrete as hardened melted nylon droplets in their post-exposure form.

HSC-NG0-20	HSC-NG0-300	HSC-NG0-600

Fig. 36. HSC specimens containing NG after exposure to elevated temperatures.

Compressive strength tests were conducted after examining the condition of concrete specimens exposed to elevated temperatures. Fig. 37 shows the failure patterns of both heat-exposed and unexposed concrete specimens after the compressive strength tests. For the unheated specimens (at ambient temperature), audible cracking sounds were clearly heard when the compressive stress approached its peak value (at stress levels above approximately $0.9f_c$), although no visible cracks were observed beforehand. Once the peak load was reached, the failure occurred abruptly and was accompanied by loud cracking noises, such that the specimens failed within 2 to 4 seconds after the peak load. In specimens exposed to 300°C, microcracks resulting from thermal loading were visible prior to mechanical loading, and these rapidly propagated during the application of compressive stress. The development of these cracks became noticeable at stress levels above $0.6f_c$. The cracking noises were relatively faint, but the opening of crack planes was visible. Failure in these specimens occurred more gradually, with complete fracture occurring 7 to 10 seconds after the peak stress. Additionally, lateral expansion of the specimens was clearly observed after reaching peak stress. In specimens exposed to 600°C, the cracking and failure patterns closely resembled those observed in the 300°C group; however, the crack sounds were even milder, and the failure rate was slower. According to ASTM C39 [43], typical failure patterns include vertical cracks, well-formed cones at one end, or shear failures near the ends of the cylinders. In this study, as shown in Fig. 37, most specimens exhibited vertical cylindrical cracks at their ends, and well-formed conical failures were generally not observed.

As an additional visual inspection, the overall internal condition of HSC specimens containing NG exposed to elevated temperatures was evaluated after the splitting tensile strength test. Fig. 38 illustrates the interior view of all concrete specimens following this test. It can be observed that, with increasing exposure temperature, both the overall color of the specimens and the aggregate color become significantly faded and tend toward white. As previously mentioned, this phenomenon is attributed to the loss of free and surface water, as well as the dehydration of chemically bound water in the C-S-H gel. Moreover, with rising temperatures, a significant increase in internal pores is observed in specimens containing NG. This is due to the thermal decomposition of NG, which leads to the complete breakdown of the nylon granules and ultimately results in increased porosity and a more porous concrete matrix.

4.10. Microstructure

Another aspect of this study involved the microstructural analysis of heat-exposed and unexposed high-strength concrete specimens containing 10% replacement of NG, following the compressive strength test. Scanning Electron Microscopy (SEM) was conducted on a polished thin section measuring 20 × 15 mm, prepared by cutting a portion of the concrete specimen. Fig. 39 presents the SEM images of high-strength concrete specimens containing 10% NG after exposure to 20, 300, and 600°C, where a significant presence of white sponge-like structures can be observed at elevated temperatures. Fig. 39-a shows the SEM images of the specimens at 20°C. At this ambient temperature, nylon granules are clearly visible, and the number of micro-cracks and pores is significantly lower than in heat-exposed specimens. Fig. 39-b corresponds to the SEM images of specimens exposed to 300°C. The image reveals

a notable increase in porosity attributed to the evaporation of bound water and the degradation of the cement paste at elevated temperatures. These changes could be due to the thermal deformation of cement crystals, dehydration of CH crystals, and the decomposition of the C-S-H gel, which lead to structural degradation and increased porosity. Additionally, partial decomposition of nylon granules contributes to the observed high porosity in this group. Fig. 39-c displays SEM images of specimens exposed to 600°C. At this temperature, the progressive loss of chemically bound water has further exposed the microstructure of CH crystals and the C-S-H gel, making the expansion of sponge-like structures more visible (see the large white masses in Fig. 35c). Moreover, this group exhibits the highest degree of porosity and microcracking, which can be attributed to the complete decomposition of nylon granules, dehydration of CH crystals, and breakdown of the C-S-H structure. As the nylon granules have surpassed their decomposition temperature (based on the TGA results shown in Fig. 4), large voids are apparent in the image, corresponding to the evaporation of nylon particles.

Specimen	20 °C	300 °C	600 °C
HSC-NG0®			
HSC-NG10			
HSC-NG20			

Fig. 37. Failure mode of specimens under compressive loading.

Specimen	20 °C	300 °C	600 °C
HSC-NG0®			
HSC-NG10			
HSC-NG20			
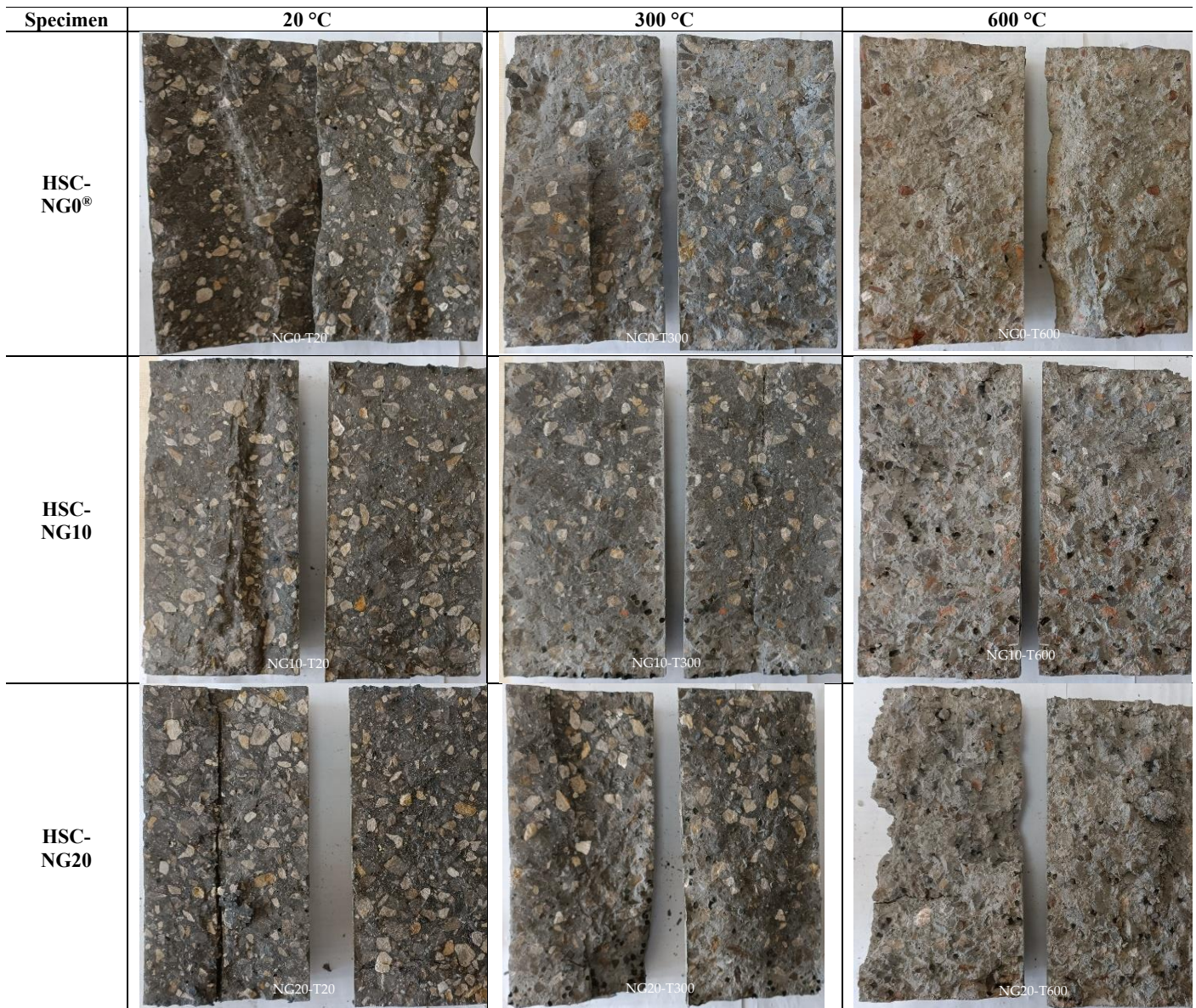
Fig. 38. Failure mode of specimens under tensile loading.

5. Conclusions

This study investigated the compressive stress-strain behavior of HSC containing NG after exposure to elevated temperatures. Furthermore, empirical relationships were developed to predict the mechanical properties of NG-incorporated high-strength concrete subjected to various temperature levels. Based on these relationships, a model was formulated to simulate the compressive stress-strain response of this type of concrete. In addition, the predicted results were compared with experimental findings as well as with the values recommended by international design codes and standards.

- Weight loss in concrete specimens increased with elevated temperatures, especially at 600°C. At 300°C, the reference specimens showed a 2% weight loss, while specimens with 10 and 20% nylon granules experienced 3 and 4% weight loss, respectively. At 600°C, weight loss rose to 8% for the reference specimens and 10 and 11% for the 10 and 20% nylon granule specimens, respectively. The highest weight loss occurred due to the complete decomposition of nylon granules. Overall, the specimens with 20% nylon replacement at 600°C showed the greatest weight loss (11%).

- Replacing natural fine aggregates with NG reduced the compressive strength of HSC, with the greatest loss (59.2%) at 20% NG at room temperature. Strength decreased further at elevated temperatures, particularly at 600 °C. Notably, specimens with 10% NG showed more stable performance above 300 °C, indicating that limited NG replacement balance thermal resilience and environmental benefits.

- Including NG as a partial replacement for natural fine aggregates reduced the splitting tensile strength of high-strength concrete HSC, with greater losses at higher temperatures. Strength decreased by up to 24.6% at room temperature with 20% NG. Upon exposure to 600 °C, all specimens showed significant strength reductions, with the 10% NG group exhibiting the lowest loss (59.2%), indicating slightly better thermal resistance.

- The inclusion of NG reduced both the initial and secant elastic moduli of HSC, with greater reductions observed at higher

temperatures. At 600 °C, modulus losses reached approximately 75% across all specimens. Notably, the lowest reduction in initial modulus occurred in the control group, while the smallest secant modulus loss was observed in specimens with 20% NG, indicating varied thermal responses depending on the modulus type and NG content.

- The peak strain of HSC increased with rising temperature, showing significant growth at 600 °C. Compared to room temperature, peak strain rose by 166.7, 46.9, and 90% for specimens with 0, 10, and 20% NG, respectively. While NG replacement generally reduced peak strain at ambient and 300 °C, all specimens exhibited notable softening and deformation under high thermal exposure.

- The ultimate strain of HSC increased with temperature, particularly at 600 °C, due to material softening and increased porosity. At room temperature and 300 °C, specimens with 10% NG showed the highest ultimate strain, while at 600 °C, the control group without NG exhibited the greatest value. These results suggest that limited NG replacement can enhance ductility at moderate temperatures, while higher temperatures promote greater deformation regardless of NG content.

- The toughness of HSC decreased with both increasing NG content and elevated temperature. Reference specimens without NG consistently exhibited the highest toughness due to their greater compressive strength. While peak strain varied slightly, the combined effect of reduced strength and increased strain at higher temperatures led to an overall decline in toughness across all specimens.

- A model was proposed to accurately represent the axial compressive stress-strain behavior of concrete containing NG at elevated temperatures. Based on empirical equations for various mechanical concrete properties, the model showed suitable agreement with experimental results, effectively capturing the changes in stress-strain behavior at different temperatures.

- Concrete exposed to elevated temperatures showed clear signs of damage, including color changes, surface cracking, and increased porosity. At 300°C and above temperatures, nylon granules softened and fully decomposed at 600°C, creating internal voids and contributing to a more porous concrete structure. The decomposed granules evaporated through surface cracks, leaving behind hardened nylon droplets on the surface.

- Compressive strength tests demonstrated that failure in specimens exposed to high temperatures occurred gradually. Cracks formed before peak stress, and failure was slower compared to unexposed specimens. Specimens exposed to 600°C exhibited milder cracking sounds and slower failure. Internal inspection revealed increased porosity and fading color caused by water loss and nylon granule decomposition.

- The microstructural analysis of high-strength concrete with 10% NG replacement showed notable changes at elevated temperatures. At 20°C, nylon granules were visible with minimal microcracking and porosity. At 300°C, increased porosity occurred due to water evaporation and partial nylon granule decomposition. At 600°C, the highest porosity and microcracking were observed, resulting from complete nylon granule decomposition, CH crystal dehydration, and C-S-H gel breakdown, with large voids indicating nylon evaporation


(a)

(b)

(c)
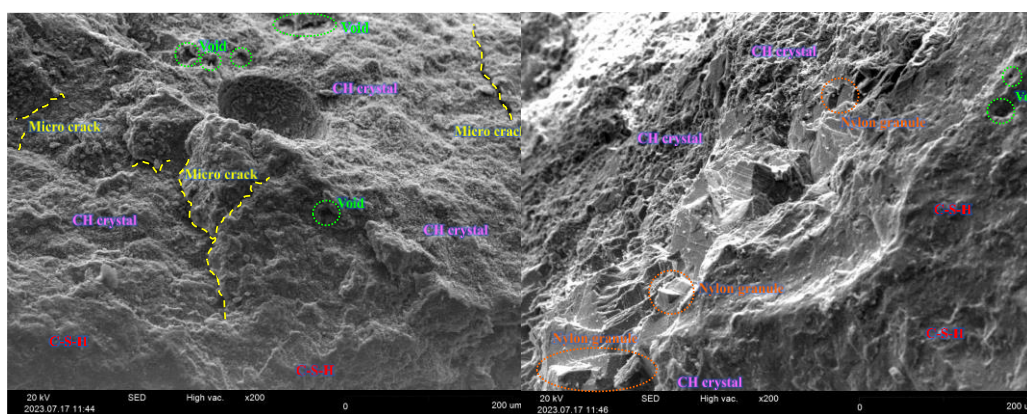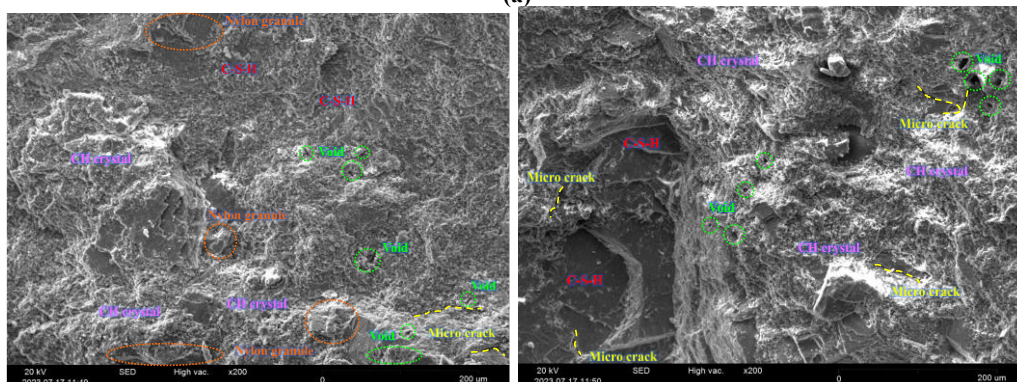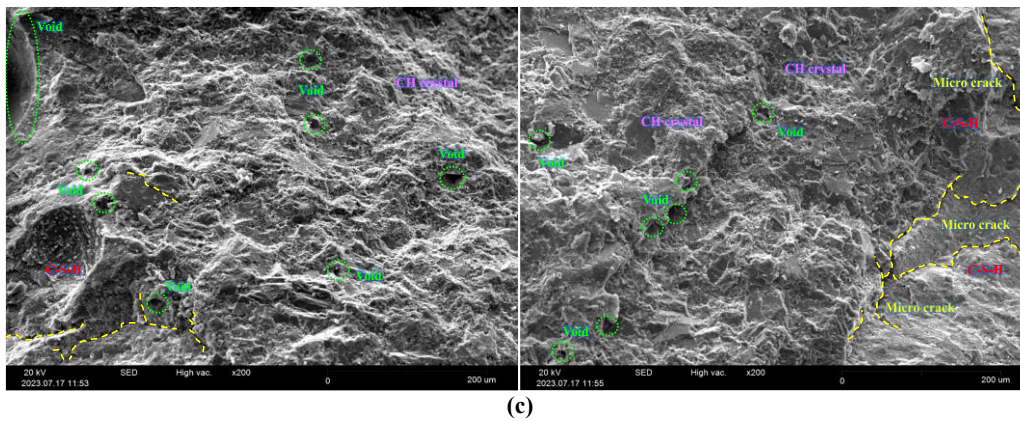
Fig. 39. SEM micrographs of heated and non-heated high-strength concrete specimens containing nylon granule: (a) SEM image of cement paste after exposure to 20 °C, (b) SEM image of cement paste after exposure to 300 °C, and (c) SEM image of cement paste after exposure to 600 °C.

Statements & declarations

Author contributions

Fariborz Sasania: Conceptualization, Investigation, Methodology, Formal analysis, Resources, Writing - Original Draft, Writing - Review & Editing.

Mahdi Nematzadeh: Conceptualization, Methodology, Formal analysis, Project administration, Supervision, Writing - Review & Editing.

Maryam Asadi: Investigation, Visualization, Validation, Formal analysis, Resources, Writing - Original Draft, Writing - Review & Editing.

Arman Aminian: Investigation, Visualization, Validation, Formal analysis, Resources, Writing - Original Draft, Writing - Review & Editing.

Data availability

The data presented in this study will be available on interested request from the corresponding author.

Declarations

The authors declare no conflict of interes.

References

[1]   Li, D., Zhuge, Y., Gravina, R., Mills, J. E. Compressive Stress Strain Behavior of Crumb Rubber Concrete (CRC) and Application in Reinforced CRC Slab. Construction and Building Materials, 2018; 166: 745–759. doi:10.1016/j.conbuildmat.2018.01.142.

[2]   Zarei, M., Rahmani, Z., Zahedi, M., Nasrollahi, M. Technical, Economic, and Environmental Investigation of the Effects of Rubber Powder Additive on Asphalt Mixtures. Journal of Transportation Engineering, Part B: Pavements, 2020; 146 (1): 04019039. doi:10.1061/jpeodx.0000142.

[3]   Tayebi, M., Nematzadeh, M. Post-Fire Flexural Performance and Microstructure of Steel Fiber-Reinforced Concrete with Recycled Nylon Granules and Zeolite Substitution. Structures, 2021; 33: 2301–2316. doi:10.1016/j.istruc.2021.05.080.

[4]   Thomas, B. S., Chandra Gupta, R. Properties of High Strength Concrete Containing Scrap Tire Rubber. Journal of Cleaner Production, 2016; 113: 86–92. doi:10.1016/j.jclepro.2015.11.019.

[5]   Gupta, T., Chaudhary, S., Sharma, R. K. Assessment of Mechanical and Durability Properties of Concrete Containing Waste Rubber Tire as Fine Aggregate. Construction and Building Materials, 2014; 73: 562–574. doi:10.1016/j.conbuildmat.2014.09.102.

[6]   Pelisser, F., Zavarise, N., Longo, T. A., Bernardin, A. M. Concrete Made with Recycled Tire Rubber: Effect of Alkaline Activation and Silica Fume Addition. Journal of Cleaner Production, 2011; 19 (6–7): 757–763. doi:10.1016/j.jclepro.2010.11.014.

[7]   Mousavimehr, M., Nematzadeh, M. Predicting Post-Fire Behavior of Crumb Rubber Aggregate Concrete. Construction and Building Materials, 2019; 229. doi:10.1016/j.conbuildmat.2019.116834.

[8]   Wang, H. Y., Chen, B. T., Wu, Y. W. A Study of the Fresh Properties of Controlled Low-Strength Rubber Lightweight Aggregate Concrete (CLSRLC). Construction and Building Materials, 2013; 41: 526–531. doi:10.1016/j.conbuildmat.2012.11.113.

[9] Al-Tayeb, M. M., Abu Bakar, B. H., Akil, H. M., Ismail, H. Performance of Rubberized and Hybrid Rubberized Concrete Structures under Static and Impact Load Conditions. Experimental Mechanics, 2013; 53 (3): 377–384. doi:10.1007/s11340-012-9651-z.

[10] Yung, W. H., Yung, L. C., Hua, L. H. A Study of the Durability Properties of Waste Tire Rubber Applied to Self-Compacting Concrete. Construction and Building Materials, 2013; 41: 665–672. doi:10.1016/j.conbuildmat.2012.11.019.

[11] Yilmaz, A., Degirmenci, N. Possibility of Using Waste Tire Rubber and Fly Ash with Portland Cement as Construction Materials. Waste Management, 2009; 29 (5): 1541–1546. doi:10.1016/j.wasman.2008.11.002.

[12] Nematzadeh, M., Mousavimehr, M. Residual Compressive Stress–Strain Relationship for Hybrid Recycled PET–Crumb Rubber Aggregate Concrete after Exposure to Elevated Temperatures. Journal of Materials in Civil Engineering, 2019; 31 (8). doi:10.1061/(asce)mt.1943-5533.0002749.

[13] Gjørv O. E. High-strength concrete. Developments in the Formulation and Reinforcement of Concrete. 2008. Woodhead Publishing, Sawston, United Kingdom. doi:10.1016/b978-0-08-102616-8.00007-1.

[14] Ferreira R. M, Jalali S., Gjørv O. E. Probabilistic assessment of the durability performance of concrete structures. Engenharia Civil UM, 2004; 39-48.

[15] Singh, S., Nagar, R., Agrawal, V., Rana, A., Tiwari, A. Sustainable Utilization of Granite Cutting Waste in High Strength Concrete. Journal of Cleaner Production, 2016; 116: 223–235. doi:10.1016/j.jclepro.2015.12.110.

[16] Mohammed, A. A., Karim, S. H. Impact Strength and Mechanical Properties of High Strength Concrete Containing PET Waste Fiber. Journal of Building Engineering, 2023; 68. doi:10.1016/j.jobe.2023.106195.

[17] Bilow, D. N., Kamara, M. E. Fire and Concrete Structures. Proceedings of the 2008 Structures Congress - Structures Congress 2008: Crossing the Borders, 2008; 314: 1–10. doi:10.1061/41016(314)299.

[18] Hassanli, R., Youssf, O., Mills, J. E. Experimental Investigations of Reinforced Rubberized Concrete Structural Members. Journal of Building Engineering, 2017; 10: 149–165. doi:10.1016/j.jobe.2017.03.006.

[19] Xue, J., Shinozuka, M. Rubberized Concrete: A Green Structural Material with Enhanced Energy-Dissipation Capability. Construction and Building Materials, 2013; 42: 196–204. doi:10.1016/j.conbuildmat.2013.01.005.

[20] Karimi, A., Nematzadeh, M. Axial Compressive Performance of Steel Tube Columns Filled with Steel Fiber-Reinforced High Strength Concrete Containing Tire Aggregate after Exposure to High Temperatures. Engineering Structures, 2020; 219. doi:10.1016/j.engstruct.2020.110608.

[21] Guo, Y. C., Zhang, J. H., Chen, G. M., Xie, Z. H. Compressive Behaviour of Concrete Structures Incorporating Recycled Concrete Aggregates, Rubber Crumb and Reinforced with Steel Fibre, Subjected to Elevated Temperatures. Journal of Cleaner Production, 2014; 72: 193–203. doi:10.1016/j.jclepro.2014.02.036.

[22] Nematzadeh, M., Shahmansouri, A. A., Fakoor, M. Post-Fire Compressive Strength of Recycled PET Aggregate Concrete Reinforced with Steel Fibers: Optimization and Prediction via RSM and GEP. Construction and Building Materials, 2020; 252. doi:10.1016/j.conbuildmat.2020.119057.

[23] Gupta, T., Siddique, S., Sharma, R. K., Chaudhary, S. Effect of Elevated Temperature and Cooling Regimes on Mechanical and Durability Properties of Concrete Containing Waste Rubber Fiber. Construction and Building Materials, 2017; 137: 35–45. doi:10.1016/j.conbuildmat.2017.01.065.

[24] Marques, A. M., Correia, J. R., De Brito, J. Post-Fire Residual Mechanical Properties of Concrete Made with Recycled Rubber Aggregate. Fire Safety Journal, 2013; 58: 49–57. doi:10.1016/j.firesaf.2013.02.002.

[25] Al-Mutairi, N., Al-Rukaibi, F., Bufarsan, A. Effect of Microsilica Addition on Compressive Strength of Rubberized Concrete at Elevated Temperatures. Journal of Material Cycles and Waste Management, 2010; 12 (1): 41–49. doi:10.1007/s10163-009-0243-7.

[26] Mousa, M. I. Effect of Elevated Temperature on the Properties of Silica Fume and Recycled Rubber-Filled High Strength Concretes (RHSC). HBRC Journal, 2017; 13 (1): 1–7. doi:10.1016/j.hbrcj.2015.03.002.

[27] Nematzadeh, M., Arjomandi, A., Fakoor, M., Aminian, A., Khorshidi-Mianaei, A. Pre-and Post-Heating Bar-Concrete Bond Behavior of CFRP-Wrapped Concrete Containing Polymeric Aggregates and Steel Fibers: Experimental and Theoretical Study. Engineering Structures, 2024; 321. doi:10.1016/j.engstruct.2024.118929.

[28] Nematzadeh, M., Hosseini, S. A., Ozbakkaloglu, T. The Combined Effect of Crumb Rubber Aggregates and Steel Fibers on Shear Behavior of GFRP Bar-Reinforced High-Strength Concrete Beams. Journal of Building Engineering, 2021; 44. doi:10.1016/j.jobe.2021.102981.

[29] American Concrete Institute (ACI). ACI 216R-89: Guide for determining the fire endurance of concrete elements. Farmington Hills (MI): ACI; 1989.

[30] American Society of Civil Engineers (ASCE). Structural fire protection. Reston (VA): ASCE; 1992. doi:10.1061/9780872628885.

[31] European Committee for Standardization (CEN). EN 1994-1-2: Design of composite steel and concrete structures – Part 1-2: General

rules for structural fire design. Brussels (BE): CEN; 2004.

[32] European Committee for Standardization (CEN). EN 1992-1-2: Design of concrete structures – Part 1-2: General rules – Structural fire design. Brussels (BE): CEN; 2004.

[33] Comité Euro-International du Béton (CEB). Fire design of concrete structures – in accordance with CEB/FIP Model Code 90. Lausanne (CH): CEB; 1991.

[34] ASTM International. ASTM C150-07: Standard specification for Portland cement. West Conshohocken (PA): ASTM International; 2012. doi:10.1520/C0150-07.

[35] ASTM International. ASTM C33/C33M-16: Standard specification for concrete aggregates. West Conshohocken (PA): ASTM International; 2016. doi:10.1520/C0033_C0033M-16.

[36] ASTM International. ASTM C128-12: Standard test method for density, relative density (specific gravity), and absorption of fine aggregate. West Conshohocken (PA): ASTM International; 2015. doi:10.1520/C0128-07A.

[37] American Concrete Institute (ACI). ACI 211.1-91: Standard practice for selecting proportions for normal, heavyweight, and mass concrete. Farmington Hills (MI): ACI; 2008.

[38] ASTM International. ASTM C143/C143M-10a: Standard test method for slump of hydraulic-cement concrete. West Conshohocken (PA): ASTM International; 2012. doi:10.1520/C0143_C0143M-10A.

[39] ASTM International. ASTM C192/C192M-14: Standard practice for making and curing concrete test specimens in the laboratory. West Conshohocken (PA): ASTM International; 2015. doi:10.1520/C0192_C0192M-14.

[40] International Organization for Standardization (ISO). ISO 834-1:1999: Fire resistance tests – Elements of building construction – Part 1: General requirements. Geneva (CH): ISO; 1999.

[41] Manzoor, T., Bhat, J. A., Shah, A. H. Performance of Geopolymer Concrete at Elevated Temperature − A Critical Review. Construction and Building Materials, 2024; 420. doi:10.1016/j.conbuildmat.2024.135578.

[42] Babalola, O. E., Awoyera, P. O., Le, D. H., Bendezú Romero, L. M. A Review of Residual Strength Properties of Normal and High Strength Concrete Exposed to Elevated Temperatures: Impact of Materials Modification on Behaviour of Concrete Composite. Construction and Building Materials, 2021; 296. doi:10.1016/j.conbuildmat.2021.123448.

[43] ASTM International. ASTM C39/C39M-14: Standard test method for compressive strength of cylindrical concrete specimens. West Conshohocken (PA): ASTM International; 2014. doi:10.1520/C0039_C0039M-14.

[44] ASTM International. ASTM C496-96: Standard test method for splitting tensile strength of cylindrical concrete specimens. West Conshohocken (PA): ASTM International; 2017. doi:10.1520/C0496-96.

[45] ASTM International. ASTM C469/C469M-10: Standard test method for static modulus of elasticity and Poisson's ratio of concrete in compression. West Conshohocken (PA): ASTM International; 2014. doi:10.1520/C0469_C0469M-10.

[46] Tayeh, B. A., Zeyad, A. M., Agwa, I. S., Amin, M. Effect of Elevated Temperatures on Mechanical Properties of Lightweight Geopolymer Concrete. Case Studies in Construction Materials, 2021; 15. doi:10.1016/j.cscm.2021.e00673.

[47] Fernandes, B., Carré, H., Mindeguia, J. C., Perlot, C., La Borderie, C. Effect of Elevated Temperatures on Concrete Made with Recycled Concrete Aggregates - An Overview. Journal of Building Engineering, 2021; 44. doi:10.1016/j.jobe.2021.103235.

[48] Tu, W., Zhang, M. Behaviour of Alkali-Activated Concrete at Elevated Temperatures: A Critical Review. Cement and Concrete Composites, 2023; 138. doi:10.1016/j.cemconcomp.2023.104961.

[49] Gesoglu, M., Güneyisi, E., Hansu, O., Ipek, S., Asaad, D. S. Influence of Waste Rubber Utilization on the Fracture and Steel-Concrete Bond Strength Properties of Concrete. Construction and Building Materials, 2015; 101: 1113–1121. doi:10.1016/j.conbuildmat.2015.10.030.

[50] Murthy, A. R. C., Palani, G. S., Iyer, N. R. State-of-the-Art Review on Fracture Analysis of Concrete Structural Components. Sadhana - Academy Proceedings in Engineering Sciences, 2009; 34 (2): 345–367. doi:10.1007/s12046-009-0014-0.

[51] Yesilata, B., Isiker, Y., Turgut, P. Thermal Insulation Enhancement in Concretes by Adding Waste PET and Rubber Pieces. Construction and Building Materials, 2009; 23 (5): 1878–1882. doi:10.1016/j.conbuildmat.2008.09.014.

[52] Fawzy, H., Mustafa, S., Abd El Badie, A. Effect of Elevated Temperature on Concrete Containing Waste Tires Rubber. The Egyptian International Journal of Engineering Sciences and Technology, 2020; 29 (1): 1–13. doi:10.21608/eijest.2020.97315.

[53] Zheng, L., Huo, X. S., Yuan, Y. Strength, Modulus of Elasticity, and Brittleness Index of Rubberized Concrete. Journal of Materials in Civil Engineering, 2008; 20 (11): 692–699. doi:10.1061/(asce)0899-1561(2008)20:11(692).

[54] Correia, J. R., Lima, J. S., De Brito, J. Post-Fire Mechanical Performance of Concrete Made with Selected Plastic Waste Aggregates. Cement and Concrete Composites, 2014; 53: 187–199. doi:10.1016/j.cemconcomp.2014.07.004.

[55] Abdullah, W., AbdulKadir, M., Muhammad, M. Effect of High Temperature on Mechanical Properties of Rubberized Concrete Using

Recycled Tire Rubber as Fine Aggregate Replacement. Engineering and Technology Journal, 2018; 36 (8A): 906–913. doi:10.30684/etj.36.8a.10.

[56] Beushausen, H., Dittmer, T. The Influence of Aggregate Type on the Strength and Elastic Modulus of High Strength Concrete. Construction and Building Materials, 2015; 74: 132–139. doi:10.1016/j.conbuildmat.2014.08.055.

[57] Georgali, B., Tsakiridis, P. E. Microstructure of Fire-Damaged Concrete. A Case Study. Cement and Concrete Composites, 2005; 27 (2): 255–259. doi:10.1016/j.cemconcomp.2004.02.022.

[58] Huang, Z., Liew, J. Y. R., Li, W. Evaluation of Compressive Behavior of Ultra-Lightweight Cement Composite after Elevated Temperature Exposure. Construction and Building Materials, 2017; 148: 579–589. doi:10.1016/j.conbuildmat.2017.04.121.

[59] Zheng, W., Luo, B., Wang, Y. Stress–Strain Relationship of Steel-Fibre Reinforced Reactive Powder Concrete at Elevated Temperatures. Materials and Structures/Materiaux et Constructions, 2015; 48 (7): 2299–2314. doi:10.1617/s11527-014-0312-9.

[60] Akbarzadeh Bengar, H., Shahmansouri, A. A., Akkas Zangebari Sabet, N., Kabirifar, K., W.Y. Tam, V. Impact of Elevated Temperatures on the Structural Performance of Recycled Rubber Concrete: Experimental and Mathematical Modeling. Construction and Building Materials, 2020; 255. doi:10.1016/j.conbuildmat.2020.119374.

[61] Chen, G. M., He, Y. H., Yang, H., Chen, J. F., Guo, Y. C. Compressive Behavior of Steel Fiber Reinforced Recycled Aggregate Concrete after Exposure to Elevated Temperatures. Construction and Building Materials, 2014; 71: 1–15. doi:10.1016/j.conbuildmat.2014.08.012.

[62] Sheikh, S., Uzumeri, S. M. Analytical Model for Concrete Confinement in Tied Columns. Journal of the Structural Division, 1982; 108 (ST12): 2703–2722. doi:10.1061/jsdeag.0006100.

[63] Frangou, M., Pilakoutas, K., Dritsos, S. Structural Repair/Strengthening of RC Columns. Construction and Building Materials, 1995; 9 (5): 259–266. doi:10.1016/0950-0618(95)00013-6.

[64] Tasdemir, M. A., Tasdemir, C., Akyüz, S., Jefferson, A. D., Lydon, F. D., Barr, B. I. G. Evaluation of Strains at Peak Stresses in Concrete: A Three-Phase Composite Model Approach. Cement and Concrete Composites, 1998; 20 (4): 301–318. doi:10.1016/S0958-9465(98)00012-2.

[65] Nataraja, M. C., Dhang, N., Gupta, A. P. Stress-Strain Curves for Steel-Fiber Reinforced Concrete under Compression. Cement and Concrete Composites, 1999; 21 (5–6): 383–390. doi:10.1016/S0958-9465(99)00021-9.

[66] Nematzadeh, M., Salari, A., Ghadami, J., Naghipour, M. Stress-Strain Behavior of Freshly Compressed Concrete under Axial Compression with a Practical Equation. Construction and Building Materials, 2016; 115: 402–423. doi:10.1016/j.conbuildmat.2016.04.045.